AFRL-AFOSR-UK-TR-2013-0063

Search and Characterization of Optical Ceramics and Crystals for Diode-pumped Laser Oscillations

Professor Tasoltan Basiev

Russian Academy of Sciences
Laser Materials and Technologies Research Center
of General Physics Institute
38 Vavilov Street
Moscow, 117942 Russia

EOARD CRDF 06-9001 / CRDF RUP2-1517-MO-06

Report Date: April 2013

Final Report from 15 June 2007 to 15 June 2012

Air Force Research Laboratory
Air Force Office of Scientific Research
European Office of Aerospace Research and Development
Unit 4515, APO AE 09421-4515

REPORT DOCUMENTATION PAGE

Form Approved OMB No. 0704-0188

1. REPORT DATE *(DD-MM-YYYY)*	2. REPORT TYPE	3. DATES COVERED *(From – To)*
21 April 2012	Final Report	15 June 2007 – 15 June 2012

4. TITLE AND SUBTITLE

Search and Characterization of Optical Ceramics and Crystals for Diode-pumped Laser Oscillations

5a. CONTRACT NUMBER

FA8655-03-D-0001 0034

5b. GRANT NUMBER

CRDF 06-9001 / CRDF RUP2-1517-MO-06

5c. PROGRAM ELEMENT NUMBER

61102F

6. AUTHOR(S)

Professor Tasoltan Basiev

5d. PROJECT NUMBER

5d. TASK NUMBER

5e. WORK UNIT NUMBER

7. PERFORMING ORGANIZATION NAME(S) AND ADDRESS(ES)

Russian Academy of Sciences
Laser Materials and Technologies Research Center of General Physics Institute
38 Vavilov Street
Moscow, 117942 Russia

8. PERFORMING ORGANIZATION REPORT NUMBER

N/A

9. SPONSORING/MONITORING AGENCY NAME(S) AND ADDRESS(ES)

EOARD
Unit 4515 BOX 14
APO AE 09421

10. SPONSOR/MONITOR'S ACRONYM(S)

AFRL/AFOSR/IOE (EOARD)

11. SPONSOR/MONITOR'S REPORT NUMBER(S)

AFRL-AFOSR-UK-TR-2013-0063

12. DISTRIBUTION/AVAILABILITY STATEMENT

Distribution A: Approved for public release; distribution is unlimited.

13. SUPPLEMENTARY NOTES

14. ABSTRACT

The hot pressing formation technique from initial single crystals was optimized to enable obtainment of stable high optical ceramics from simple fluorides and their solid solutions doped with different RE3+ ions. The spectroscopic properties of Yb3+ ions in fluoride ceramics of different compositions were investigated and the advantages of fluoride hosts to include a long upper laser level lifetime as well as a low minimal pumping intensity were demonstrated. The possibility of manipulating the spectroscopic and laser properties through the usage of different fluoride hosts was demonstrated and different tuning ranges for Yb3+ ions were realized. A slope efficiency up to 45% with respect to absorbed pump was demonstrated for the CaF2-SrF2:Yb3+ solid solution. Fluoride CaF2:Yb3+ ceramics were prepared by hot pressing single crystals and by the standard technique from powder and laser oscillations were obtained. Due to the low quantum defect of Yb3+ ions in CaF2:Yb3+ (30%), efficient CW operation was obtained without cooling the ceramic sample. Neodymium doped laser ceramics were obtained and the spectroscopic properties of different optical centers were determined. It was shown that selective excitation of non-quenched tetragonal optical centers resulted in a shorter oscillation wavelength with higher slope efficiency. It was also demonstrated that by using solid solutions of SrF2-LaF3, problems of low quantum yield arising from Nd-Nd paired optical centers were diminished enabling high oscillation efficiencies regardless of the laser diode pump wavelength. Efficient Nd3+ laser oscillations with a slope efficiency up to ~20% were realized under selective laser diode pumping in SrF2:Nd3+ fluoride and SrF2-LaF3:Nd3+ solid solution laser ceramics. For an optimized SrF2:Nd3+ crystal, a ~30% slope efficiency with respect to absorbed laser diode pump power was obtained which was comparable with the best result of 40% obtained for a YAG:Nd3+ crystal. High optical quality SrF2:Pr3+ ceramics were developed and optical losses in ceramics at the visible wavelength of 639 nm were evaluated to be on the order of the optical losses in the near infrared. Visible oscillations in red were realized in SrF2:Pr3+ ceramics with slope efficiencies of up to 9%. Praseodymium paired optical centers were shown not to be quenched and therefore do not strongly affect the lasing efficiency. Lanthanum co-doped solid solutions containing praseodymium were shown to demonstrate oscillation properties close to those of the LaF3 crystal while preserving of the cubic structure necessary for ceramics formation.

15. SUBJECT TERMS

EOARD, solid state lasers, ceramic, laser materials

16. SECURITY CLASSIFICATION OF:			17. LIMITATION OF ABSTRACT	18, NUMBER OF PAGES	19a. NAME OF RESPONSIBLE PERSON
a. REPORT	b. ABSTRACT	c. THIS PAGE			John D. Gonglewski
UNCLAS	UNCLAS	UNCLAS	SAR	38	19b. TELEPHONE NUMBER *(Include area code)* +44 (0)1895 616007

RUSSIAN ACADEMY OF SCIENCES

LASER MATERIALS AND TECHNOLOGIES RESEARCH CENTER

OF GENERAL PHYSICS INSTITUTE

Search and Characterization of Optical Ceramics and Crystals for Diode-pumped Laser Oscillations

Final report

Contract EOARD / CRDF # RUP 2–1517–MO–06

April, 2012

Moscow, Russia

1. Fluoride materials.

In recent years much attention has been paid to the development of laser hosts based on fluoride materials due to their advantages over well known oxide materials. Fluorides are characterized by a sufficiently shorter phonon spectrum as compared to oxide materials, resulting in a much weaker multiphonon relaxation which allows the obtainment of oscillations with a high optical efficiency and minimal thermal losses. Because the lifetimes of rare-earth ions in fluoride crystals are several times longer than the analogous lifetimes in oxide crystals, the development of pulsed laser amplifiers is simplified. In addition, the usage of cheaper laser diode pumping sources containing fewer laser diodes with much longer pump pulses is enabled. In addition, the lower linear and nonlinear refraction indexes for fluorides is quite unique and is extremely important for the development of laser systems. The large bandgap and small Raman gain coefficient also allows one to minimize many parasitic effects and losses. In addition, fluorides can be easily doped with a rather high level of active rare earth ions (up to 10^{21} cm^{-3}), have good mechanical properties, high moisture resistance (non-hydroscopic) and high thermal conductivity.

2. Development of fluoride ceramics.

Preliminary investigation into the development of techniques to create fluoride ceramics has shown that the main principles and approaches suitable for the development of oxide ceramics could not be applied for fluorides. Unlike oxides, in case of fluorides, the substitution of divalent cations into the matrix is both heterovalent due to the trivalent state of the impurity rare-earth ions as well as heterostructural since rare-earth doped fluorides have a hexagonal structure even though the matrix is cubic. This results in a very poor diffusion of RE^{3+} ions (RE = rare earth) into the matrix during ceramics formation and necessitates finding an approach to obtain RE^{3+} ions in the cubic phase along with local charge compensation effectively incorporated into the fluoride matrix. This problem can be solved by two methods. The first method has been well known since 1964 when the first CaF_2:Dy^{2+} ceramics were developed by grinding a doped single crystal into a sub-microsized powder followed by hot pressing of the powder to form a ceramic material. Lasing of such ceramics was successfully demonstrated [1]. Recently the same approach was utilized for the formation of the rather highly transparent ceramic, CaF_2:Yb^{3+}, which was also suitable for lasing. Even though this approach was successful, a second approach for obtaining fluoride ceramics also exists. It has been demonstrated that when a fluoride single crystal is heated to a plastic form and then uniaxially pressed up to some state, the initial single crystalline form is completely destroyed with a high quality ceramic being the result [2]. The advantage of this technique is that the initial cubic structure of the RE^{3+} doping ions along with

local charge compensation in the crystal is easily preserved in the resulting ceramic. A schematic picture of fluoride ceramics development using these two methods is shown in Fig.1.

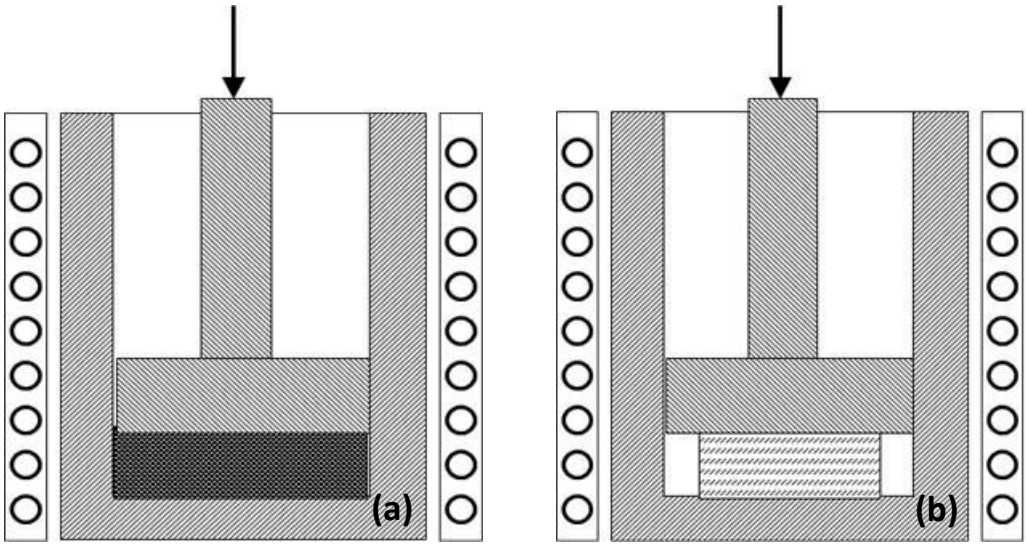

Fig.1 Fluoride ceramics development using (a) hot pressing from powder and (b) hot deformation of an initial single crystal.

The experimental setup for hot ceramics formation from fluoride single crystals is shown in Fig.2. The setup involved modification of a chamber utilized for synthesis of single crystals by the standard Bridgeman technique by inserting a specially reconstructed temperature controlled heater and pressing mechanism inside the chamber.

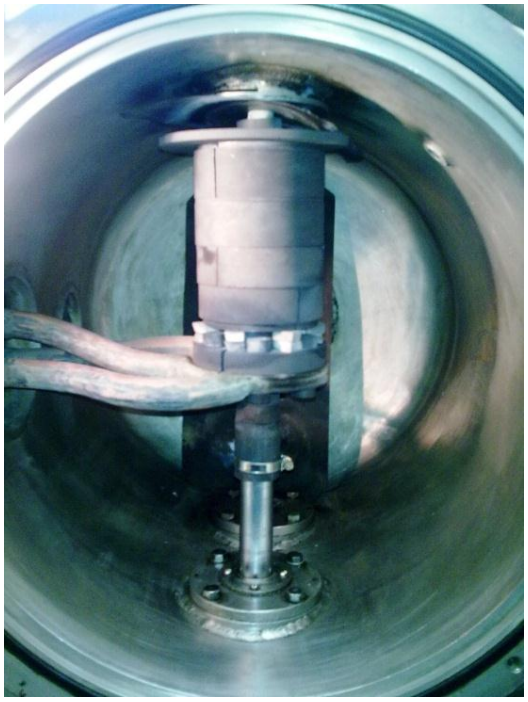

Fig.2 Modified chamber for hot formation of fluoride ceramics from single crystals.

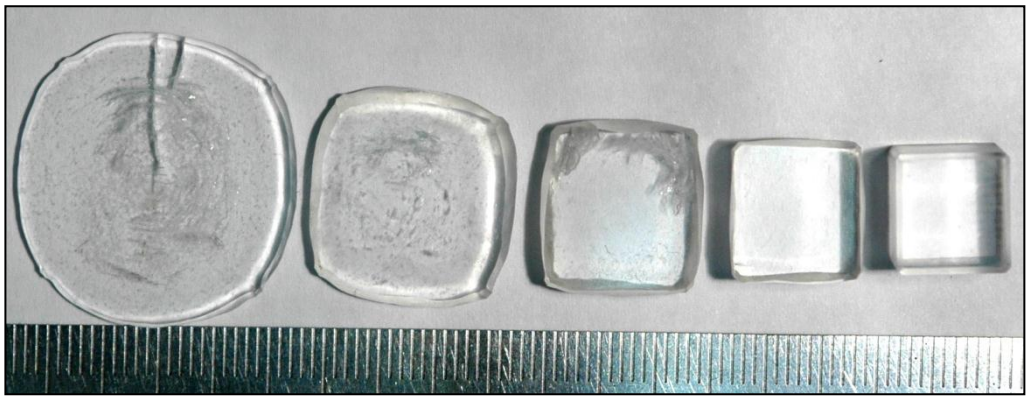

Fig.3 Different stages of hot pressed ceramics formed from single crystals depending on deformation.

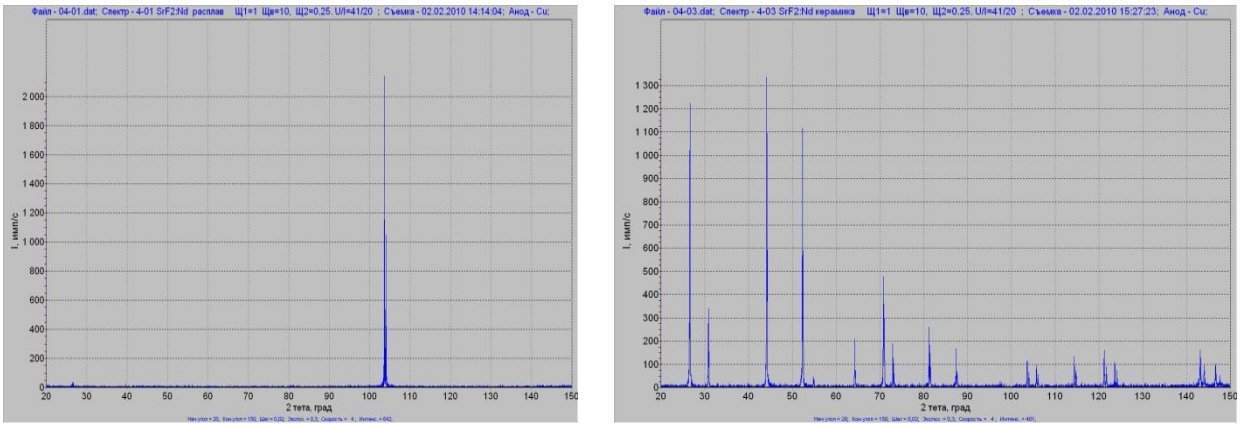

Fig.4 X-ray diagram of the initial single crystal and resulting hot pressed fluoride ceramic.

The resultant ceramics formed by hot pressing fluoride single crystals as a function of the volume of deformation is illustrated by Fig.3. By appropriate adjustment of the heating conditions and pressure, high optical quality ceramics can be produced. To validate the ceramic nature of the resulting samples, X-ray analysis was performed with the results shown in Fig.4. As can be seen from the figure, the X-ray diagram is significantly changed from a single reflection peak characteristic of the single crystal cubic structure to numerous reflection peaks characteristic of ceramic samples.

Investigations of the resulting ceramics by etched surface microscopy as well as surface electron imaging have shown that the characteristic size of the grains is about 40 μm for both methods of ceramics production. Examples of microscopic and surface electron imaging of fluoride ceramics are shown in Fig.5.

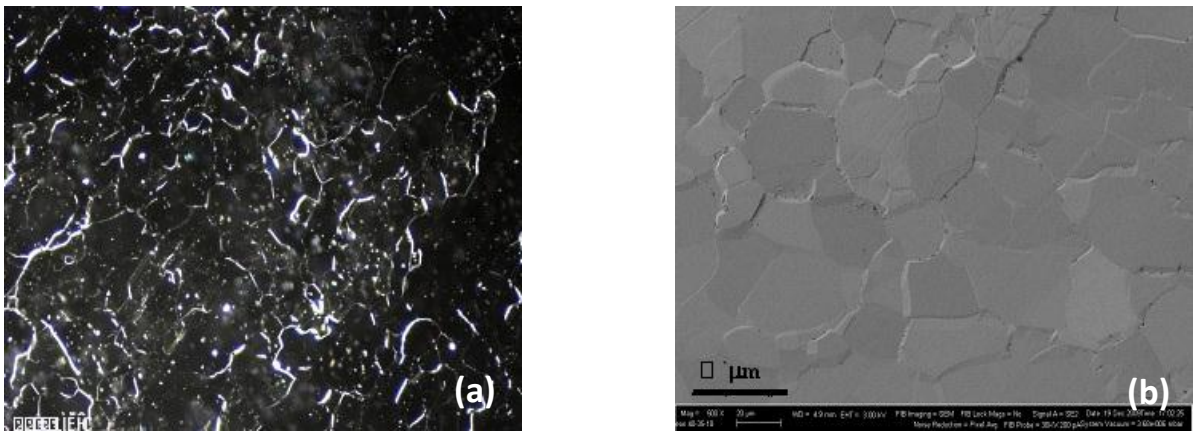

Fig.5 (a) Microphotograph of the ceramics grains and (b) electron image of the surface.

The advantages of fluoride ceramics compared to single crystal are:

- Higher fracture toughness;
- Higher microhardness;
- No cleavage planes;
- Large size;

Also for some experiments, the optical quality of the resultant ceramic material was improved relative to the initial single crystal. This is exemplified in Fig.6, where the beam of a red laser diode was passed through a specially selected low optical quality $SrF_2:Pr^{3+}$ single crystal and later passed through the ceramic material produced from this crystal.

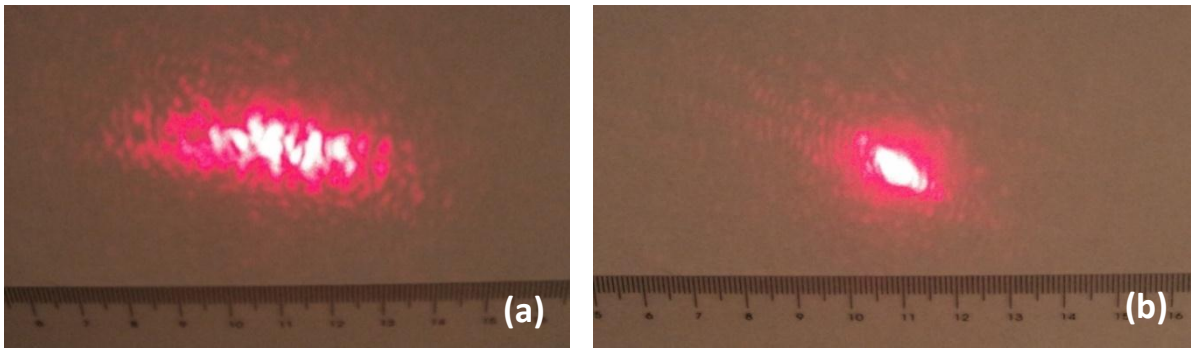

Fig. 6 Red laser diode beam passing through (a) specially selected low optical quality single crystal and (b) ceramic material produced from this single crystal by the hot pressing technique.

Examples of synthesized fluoride single crystals and resulting ceramic materials produced by the hot pressing technique are shown in Fig.7. An example of a large size $CaF_2:Yb^{3+}$ ceramic sample produced by hot pressing from a single crystal is shown in Figure 8.

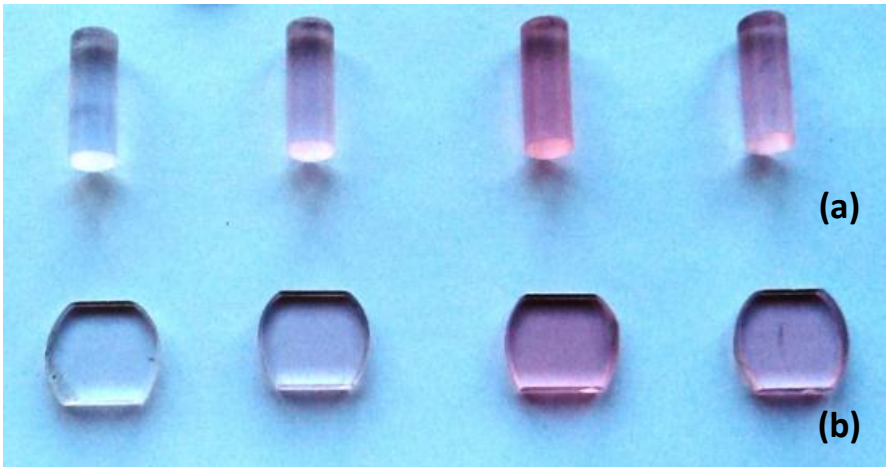

Fig.7 (a) Single crystalline samples of RE^{3+} doped fluorides and (b) samples cut from the corresponding hot pressed ceramics.

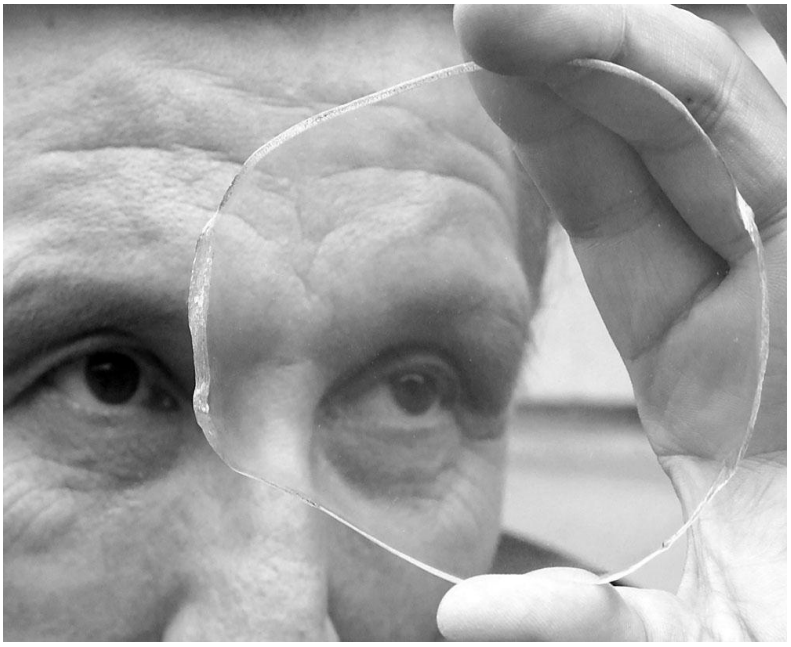

Fig.8 Laser quality large aperture CaF_2:Yb^{3+} hot pressed ceramic.

3. Optical centers of RE^{3+} ions in fluoride crystals and ceramics.

As was mentioned previously, the substitution of divalent matrix cations by RE^{3+} ions in cubic fluorides of the $Me^{2+}F_2$ type is heterovalent and thus requires compensation for excessive charge. In fluorides, this is usually accomplished through interstitial fluorine ions which are highly mobile. As was shown previously, depending on the form of the charge compensation, different types of RE^{3+} ion optical centers can be formed. In Fig.9, schematic models of the various RE^{3+} ion optical centers are presented.

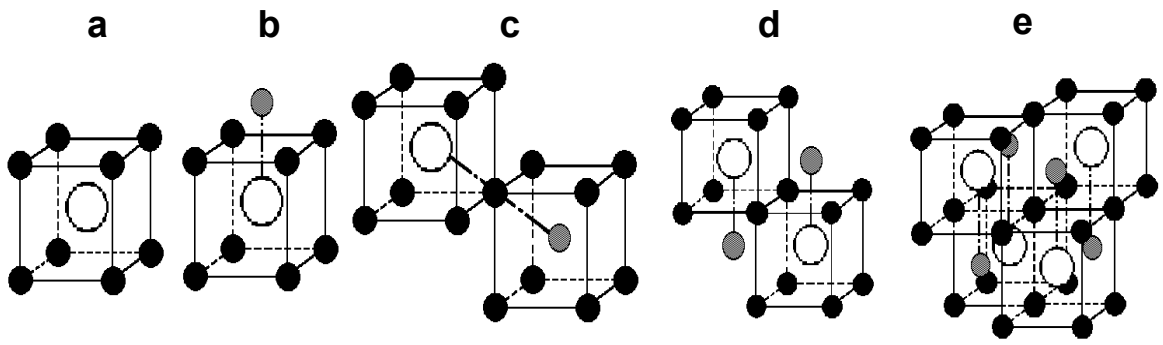

Fig.9 Structural models of Nd^{3+} centers in fluoride crystals with heterovalent substitution of divalent cations and charge compensation by interstitial fluorine ions.
a – optical center with cubic symmetry (trivalent ion without local charge compensation);
b – optical center with tetragonal symmetry (trivalent ion is compensated by interstitial fluorine in <100> direction);
c – optical center with trigonal symmetry (trivalent ion is compensated by interstitial fluorine in <111> direction);
d, e – clusters;

In the literature on the spectroscopy of Nd^{3+} optical centers, the simplest types of centers usually have special short-names for identification. Thus, an optical center with cubic symmetry (type *a* in Fig.9) is referred to as a simple cubic center. An optical center with high (close too cubic one) tetragonal symmetry (type *b* in Fig.9) is often called an L-center and the simplest clustered center formed by a pair of neighboring RE^{3+} ions (type *d* in Fig.9) is referred to as a paired M-center.

4. Yb^{3+} ions doped fluoride crystals and ceramics.

Investigation of the spectroscopic properties of Yb^{3+} ions in simple fluorides has shown that the formation of RE^{3+} optical centers as well as the resultant set of optical centers can differ for the same RE^{3+} ion in different matrixes. As an example, in Fig.10, the absorption and fluorescence spectra for different optical centers of Yb^{3+} ions in SrF_2 and CaF_2 crystals are shown. As can be seen from the figure, two types of optical centers (namely cubic centers and low symmetry paired centers) are formed in SrF_2 while in the CaF_2 crystal, three types of optical centers (namely cubic centers, low symmetry paired centers, and tetragonal optical centers) are observed.

It is known that electro-dipole transitions between 4f states in RE^{3+} ions are parity forbidden but could be partially allowed due to admixture from states having another parity (for example, the 5d state). This could be accomplished by a non-centrosymmetric local crystal field where the lower symmetry of the local crystal field results in stronger admixture of the wave functions of another parity state and thus higher probability for electronic transitions in RE^{3+} ions. Due to the

high local symmetry characteristic of cubic optical centers, the electronic transitions are slightly allowed resulting in long lifetimes of the electronic levels as well as very narrow absorption and fluorescence lines.

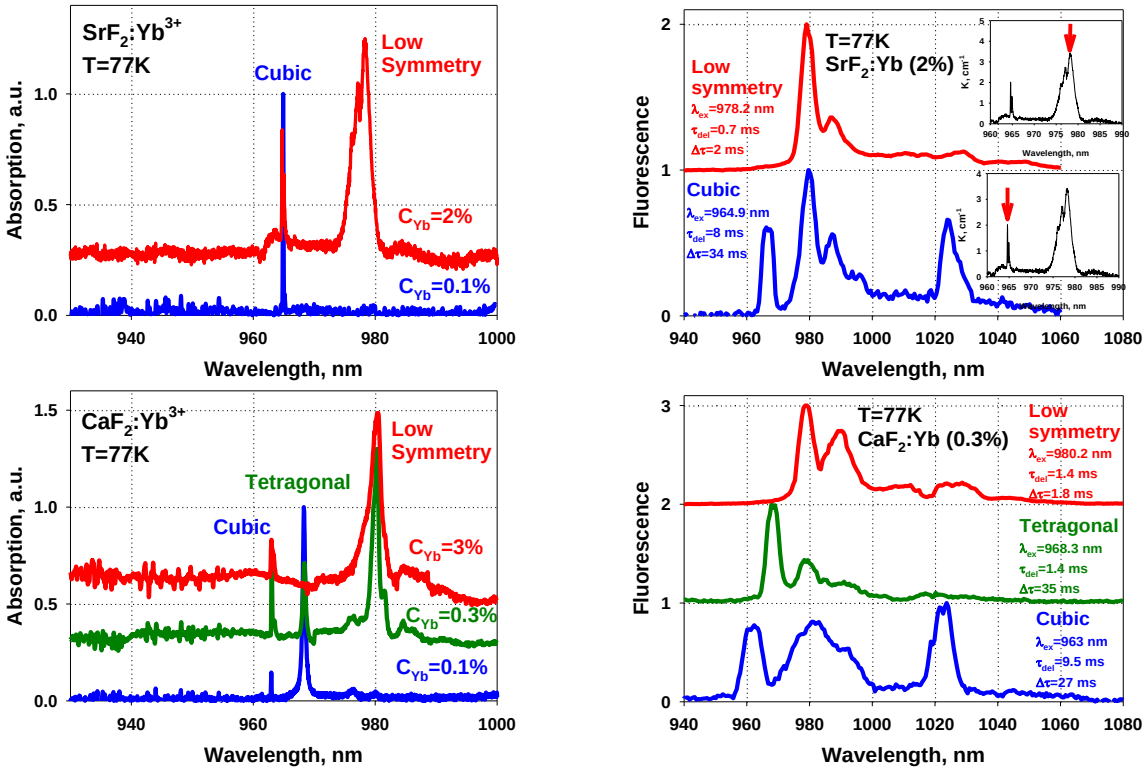

Fig.10 Absorption and fluorescence (time and spectrally resolved) spectra of different types of optical centers in SrF_2 and CaF_2 crystals.

As can be seen from the high resolution low temperature absorption spectra in Fig.10, the absorption lines of the cubic Yb^{3+} centers are very narrow, the absorption lines of the slightly lower symmetry tetragonal L-centers are a little bit broader, and the absorption lines of the low symmetry paired M-centers are much broader. Selective excitation of the individual absorption lines for each optical center, indicated on the inset in each fluorescence graph, resulted mostly in fluorescence of the selected optical center. Due to the very low emission cross sections (the transitions were slightly allowed) of cubic centers, the fluorescence signal was weak and good spectral resolution was unobtainable. That's why the fluorescence lines attributed to the cubic Yb^{3+} centers (two sideband fluorescence peaks at ~970 nm and ~1025 nm) have a larger width, determined by the spectral resolution of the measuring system, relative to that of the absorption spectrum. Even so, the spectral position of these lines could be determined quite well and the differences in the fluorescence spectra for the different types of Yb^{3+} optical centers were quite noticeable.

The decay curves of each type of optical center were measured using selective excitation along with the known positions for the fluorescence maxima of the different Yb^{3+} ion optical centers, Fig 11. As can be seen from the figure, the high symmetry cubic optical centers are characterized by long decay times on the order of 9 ms in SrF_2 and 11 ms in CaF_2 while the low symmetry, paired centers have lifetimes approximately 4-5 times shorter of about 2.3 ms in SrF_2 and 1.9 ms in CaF_2. Due to the very simple two level electronic scheme of Yb^{3+} ions, there is no way for additional losses caused by excited state absorption or cross-relaxation to occur. Thus lifetime shortening in case of Yb^{3+} ions results only from the lower symmetry of the local environment of Yb^{3+} ions. This is also seen by the rather short lifetime for Yb^{3+} tetragonal optical centers (about 2.3 ms) in CaF_2:Yb^{3+}.

From the absorption spectra in Fig.10, the concentration of low symmetry optical centers rapidly increases as the total Yb^{3+} concentration increases and for large concentrations (2-3%), this type of optical center predominates. This needs be taken into account when discussing the usage of crystalline or ceramic samples for lasing (for diode pumping, the Yb^{3+} concentration in a sample should be rather high to ensure efficient pump laser absorption at short focusing distance.

In Fig.12 the measured lifetimes of Yb^{3+} low symmetry optical centers in different simple fluorides and solid solutions are shown.

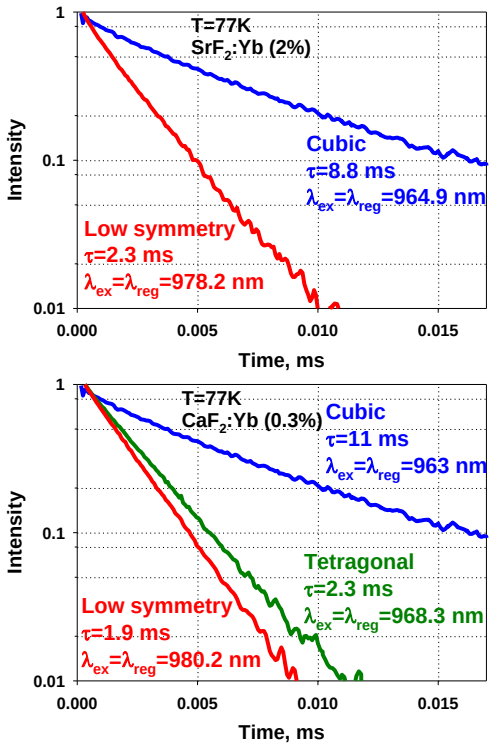

Fig.11 Decay curves of Yb^{3+} ions in different types optical centers.

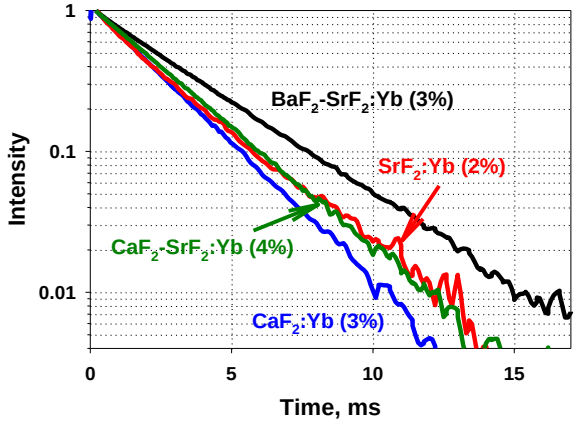

Fig.12 Decay curves of low symmetry Yb^{3+} centers in different fluorides.

As can be seen from Fig.12, the lifetime of the predominating low symmetry Yb^{3+} optical centers varies depending on the host. This is, again, due to modification of the local crystal field caused by changes in the size of the elementary cell. The elementary cell size in simple fluorides correlates with the ionic radius of the matrix cation and changes, for example, from 0.5464 nm in CaF_2 to 0.578 nm in SrF_2 because of the larger ionic radius of Sr^{2+}.

The main advantage of fluorides is the possibility of obtaining a wide range of different solid solutions. Because of this, the local environment of RE^{3+} ions could be significantly changed resulting in a variation of the spectroscopic and laser properties of the RE^{3+} ions. As an example of such variation, the absorption and emission spectra of Yb^{3+} ions at low (77K) temperature in different hosts are shown in Fig.13.

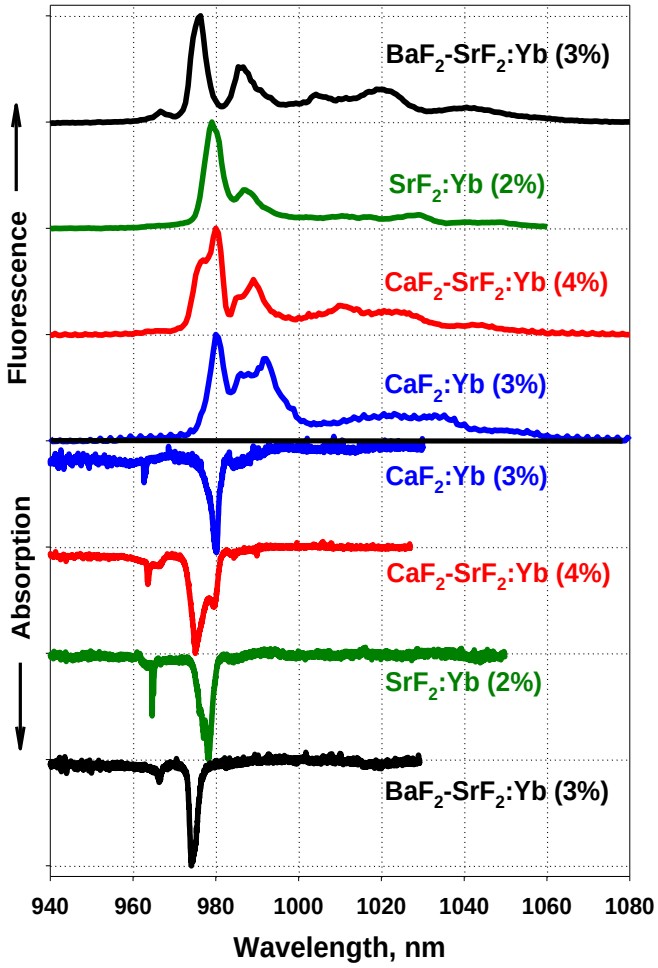

Fig.13 Variation of the absorption and emission spectra of Yb^{3+} ions on the composition of the host.

Analogous to the doping of fluoride solid solutions with Nd^{3+} ions, changes in the matrix cation results in a shift of all the absorption and fluorescence maximums of Yb^{3+} ions due to changes in the Stark splitting of the electronic levels, Fig.13. Also, because of an increase in the ionic radius

of the host cation, i.e., $r_{Ba} > r_{Sr} > r_{Ca}$, which brings changes in the elementary matrix cell dimensions and the local crystal field, the resultant Stark splitting of the levels thus results in a shift of both the absorption and fluorescence maximums to shorter wavelengths.

The room temperature absorption and emission cross-sectional spectra for the predominating low symmetry Yb^{3+} optical centers recalculated from measured absorption and emission spectra of Yb^{3+} ions in different fluoride hosts are shown in Fig.14. As can be seen in Fig.14, a small discrepancy in the absorption and emission cross-section at the zero phonon line is observed for all hosts. This is due to residual reabsorption of the fluorescence signal at the strong absorption line even though the fluorescence was measured in powder samples. As also follows from Fig.14, the highest emission cross-section is observed for the CaF_2-SrF_2 solid solution.

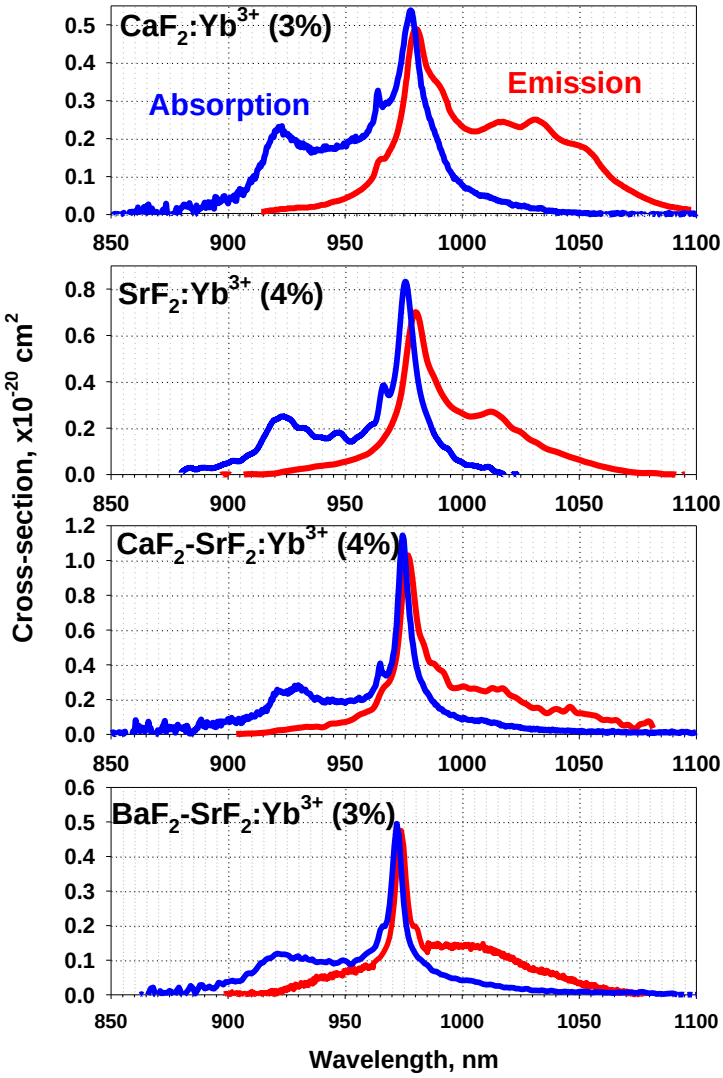

Fig.14 Absorption and emission cross-section of Yb^{3+} ions in fluoride hosts.

Lifetimes of Yb^{3+} low symmetry centers in different fluorides are summarized in Table 1 (note that the table also contains data for the well-known YAG:Yb^{3+} crystal for comparison purposes).

As can be seen from the Table, despite a shortening of the lifetimes of the lower symmetry optical centers relative to the higher symmetry cubic centers, these lifetimes are still more twice as long as the lifetime associated with the well-known YAG:Yb^{3+} crystal. Values of the emission cross sections for the different fluorides at a wavelength of 1040 nm in crystals and solid solutions are also included in the Table. As follows from the Table, the highest value for the emission cross-section was obtained for the YAG:Yb^{3+} crystal (λ=1031 nm). A value for the minimal pumping intensity was suggested in [3] as a figure of merit for fluoride hosts doped with Yb^{3+} ions:

$$I_{\min} = \frac{\sigma_{abs.\lambda osc}}{\sigma_{osc} + \sigma_{abs.\lambda osc}} \frac{h\gamma}{\sigma_{abs}\tau}$$

where $\sigma_{abs,\lambda osc}$ is the absorption cross section at the oscillation wavelength, σ_{osc} is the emission cross-section at the oscillation wavelength, σ_{abs} is the absorption cross section at the pump wavelength, and τ is the upper laser level lifetime. As can be seen from Table 1, due to low absorption losses and long lifetimes, values for the minimal pumping intensity for all fluorides presented in the table are less than the value associated with theYAG:Yb^{3+} crystal.

Table 1 Emission cross-sections and minimal pumping intensities of Yb^{3+} ions in different fluoride hosts.

Crystal	Emission cross-section, x10^{-20} см^2	Minimal Pumping Intensity, kW/см^2	LifeTime, ms (T=300K)
$Y_3Al_5O_{12}$:Yb (10%)	2.03	1.53	1.0
CaF_2:Yb (3%)	0.17	1.5	2.28
CaF_2-SrF_2:Yb (4%)	0.16	0.8	2.56
SrF_2:Yb (3%)	0.15	1.0	2.83
BaF_2-SrF_2:Yb (3%)	0.13	1.1	3.32

In Fig.15, a logarithmic plot of the measured values of the emission cross-sections versus the minimal pump intensity is presented along with additional data for other fluoride materials taken from [3]. The favorable location on the plot is top and left. The red points in Fig.15 for the SrF_2 and CaF_2-SrF_2 hosts correspond to values obtained for the shorter 1.025 nm emission wavelength. As can be seen from the plot, simple fluorides and fluoride solid solutions demonstrate one of the lowest values for minimal pumping intensity making them quite interesting for development of Yb^{3+} doped laser active media.

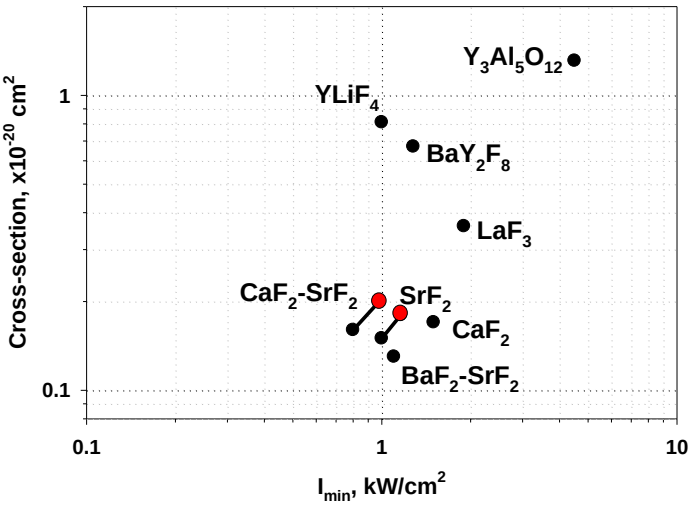

Fig.15 Emission cross-sections and minimal pump intensity values for different fluorides

The long lifetime of the upper laser level in fluorides should be useful for applications where the excitation capacity is important (for example, in power amplifiers) and will be especially good when diode pumping is utilized due to the rather low pump rate of diodes. The comparatively low emission cross-section of fluorides is also favorable in that it leads to a decrease in losses from amplified stimulated emission (ASE). Finally, clustering of Yb^{3+} ions in fluorides is positive in that the energy migration rate is decreased significantly, i.e., 6-8 times, enabling an increase in the quantum yield.

As can be seen in Fig.13, changing the matrix cation from Ca to Sr to Ba leads to a shift of both the absorption and emission spectra maxima towards shorter wavelengths. The fluoride host composition is also seen to influence the width of the fluorescence spectrum thus modifying the maximum and the range of possible oscillation wavelength tuning. The tuning curves of Yb^{3+} ions measured in CaF_2-SrF_2 and BaF_2-SrF_2 solid solutions using an intracavity Lyot filter relative to the tuning curve of SrF_2 are shown in Fig.16. As can be seen from the figure, a tuning range of 1000-1085 nm can be realized with the maximum and the shape of the tuning curve depending on the fluoride composition. Because of the shift in the fluorescence spectra, a shorter oscillation wavelength was observed for the BaF_2-SrF_2 solid solution than for the CaF_2-SrF_2 solid solution and the SrF_2 fluoride.

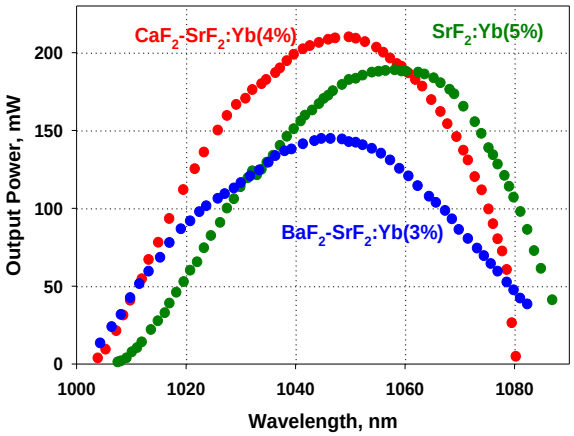

Fig.16 Tuning curves of Yb^{3+} ions in different fluoride hosts.

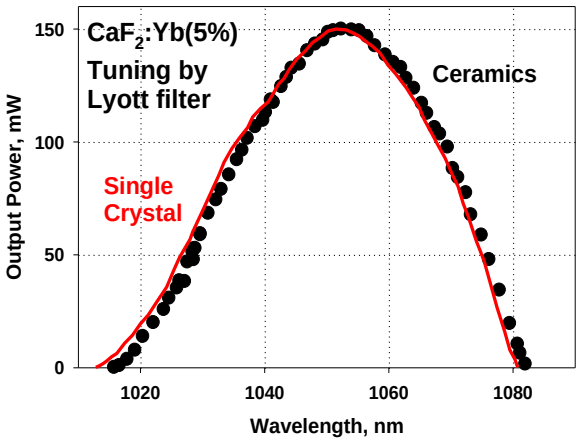

Fig.17 Comparison of the tuning curves of Yb^{3+} ions in CaF_2 single crystal and ceramics.

The tuning curves of Yb^{3+} ions in fluorides of the same composition but of different forms were measured to be practically equal. As an example in Fig.17, a comparison between the tuning curves of Yb^{3+} ions in CaF_2 single crystal and ceramics is presented. As can be seen from the figure, the difference in the maximum and the shape of the tuning curves is negligible. This demonstrates that the spectroscopic properties of RE^{3+} ions in fluoride single crystals and ceramics of the same composition are similar.

In Fig.18a, the input-output characteristics of Yb^{3+} doped single crystal and ceramic samples measured in similar conditions are presented. As can be seen from the figure, the lasing threshold and slope efficiency were similar in the case of single crystal and ceramic hosts with a slightly lower slope efficiency of 37-45% being demonstrated for the ceramic sample. As can be seen from Fig.18b, the slope efficiency for in Yb^{3+} in a CaF_2-SrF_2 solid solution was higher than for Yb^{3+} in the CaF_2 host. This superiority follows from Table 1 where the minimum pump intensities for the different fluorides were estimated. As can be seen in Table 1, a smallest value of 0.8 kW/cm^2 for the minimal pumping intensity was obtained for the CaF_2-SrF_2 solid solution.

The ability of the samples to lase was tested in the setup shown in Fig.19. The samples were pumped with a 967 nm fiber coupled (fiber core 120 μm) 10 W laser diode with single lens (5 mm focal length) placed at double the focus distance to enable translation of the image of the output fiber end into the crystal. The diode was mounted on a Peltier module which enabled adjustment of the pump wavelength through changes in the laser diode temperature. To avoid heating of the samples which were not cooled, the diode was pulsed with a pulse duration of 2-3 ms and a repetition rate of 5 Hz. The measured diameter of the pump beam near the lens focal plane is shown in Fig.20. The cavity was formed by a back flat dichroic mirror having maximum

transmission at the pump wavelength and maximum reflection within the 1000-1200 nm spectral range and a curved (curvature 50 mm) output coupler with reflectivity of 95% placed 40 mm from the back flat mirror. The corresponding reflection spectra of the mirrors are shown in Fig.21.

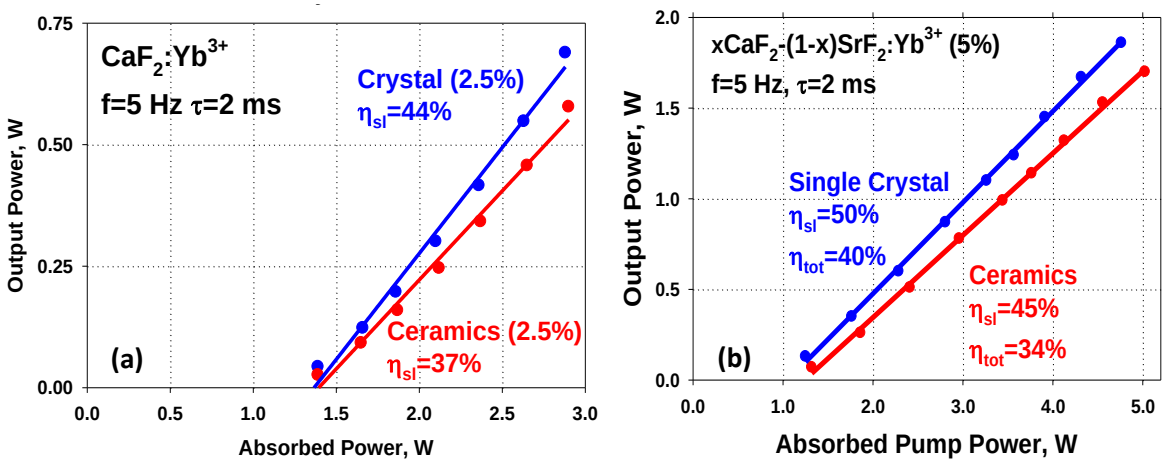

Fig.18 Input-output characteristics of Yb^{3+} ions in (a) CaF_2 and SrF_2 single crystal and ceramics measured in the same conditions, and (b) CaF_2-SrF_2 single crystal and ceramics solid solution measured in the same conditions.

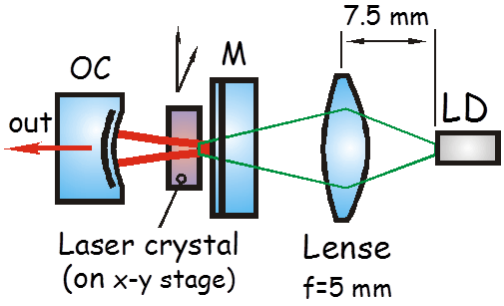

Fig.19 The schematic image of the lasing experiments setup.

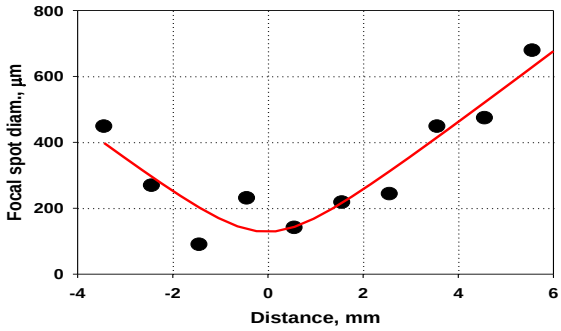

Fig.20 Pump beam diameter near the lens focus.

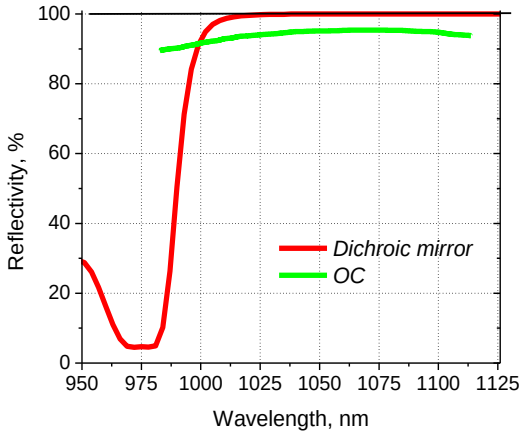

Fig.21 Reflection spectra of the flat dichroic mirror and output coupler used in the laser experiments.

In Fig.22, the input-output characteristics of both CaF_2:Yb^{3+} ceramics and single crystal are shown as a function of the reflectivity of the output mirror for similar conditions. As can be seen from the figure, the oscillation thresholds and lasing efficiencies for the single crystal and ceramics are in very good agreement. The dependencies of the oscillation threshold on the output mirror reflectivity shows equal losses of about 12% for both the crystal and ceramics which can be attributed mostly to residual absorption of the Yb^{3+}.

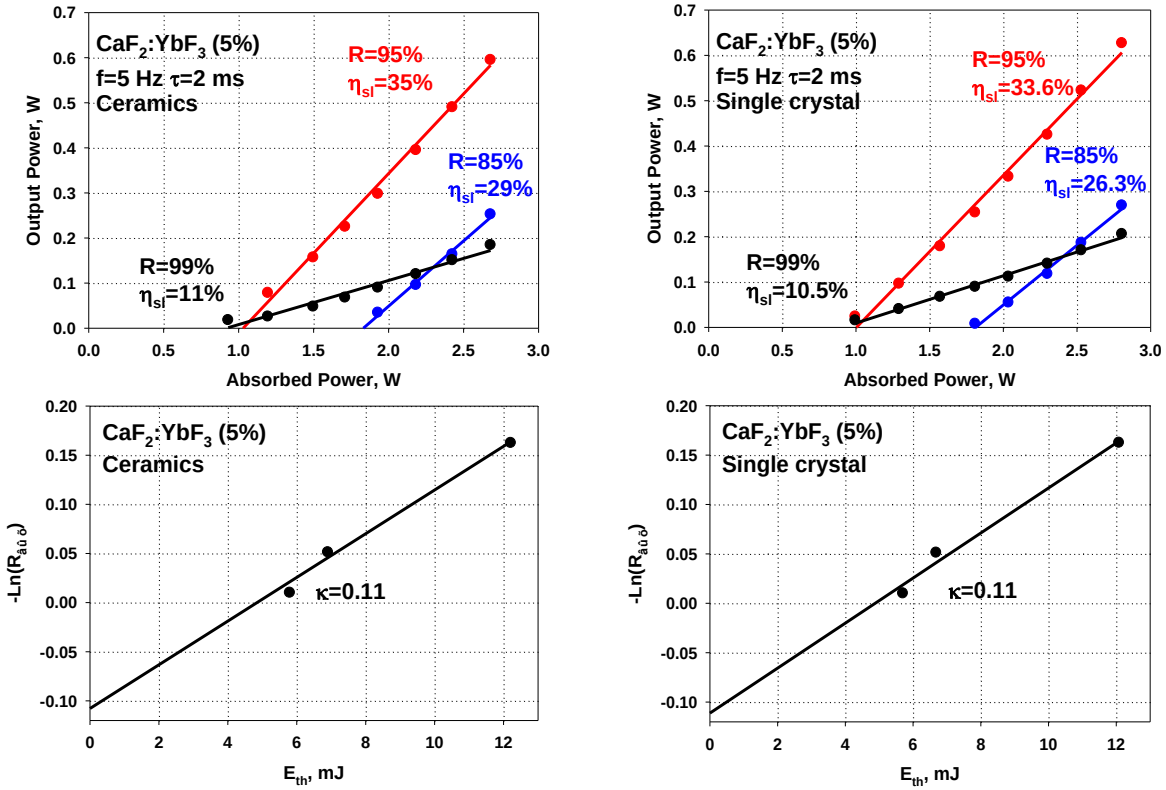

Fig.22 Oscillation properties of CaF_2:Yb^{3+} (5%) crystal and ceramics under laser diode pumping and evaluation of optical losses.

As was mentioned above, the laser experiments were performed with a pulsed laser diode to decrease heating of the samples. Because of the small quantum defect and rather high oscillation efficiency, heat generation in the Yb^{3+} doped fluoride samples was found to be rather small even without cooling. Because of low levels of heating, testing of the CaF_2:Yb^{3+} ceramics could be performed in the continuous wave (CW) mode of operation. In Fig.23, the input-output characteristics of CaF_2:Yb^{3+} ceramics in both the pulsed and CW modes of operation are shown. As can be seen from the figure, an identical slope efficiency of 30% was obtained in both cases with respect to absorbed pump power.

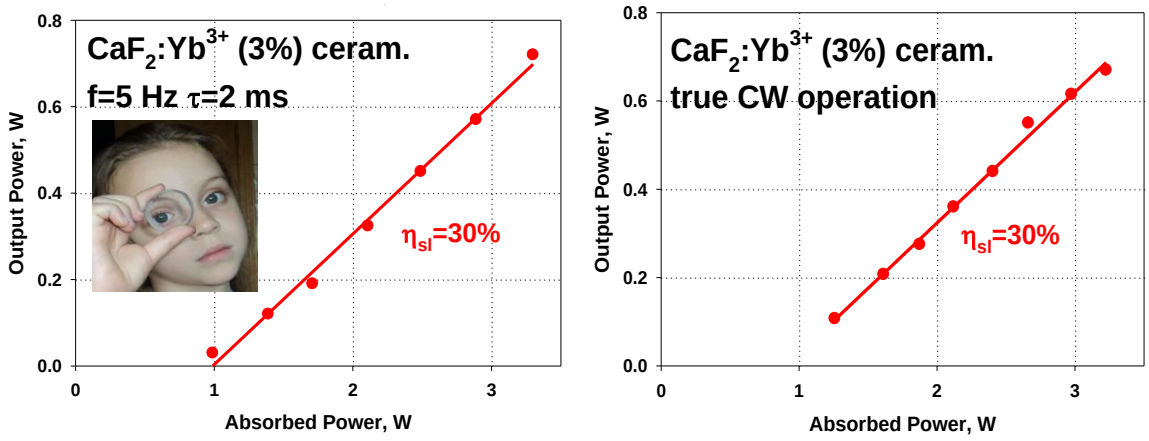

Fig.23 Comparison of $CaF_2:Yb^{3+}$ laser properties in both pulsed and CW modes of operation.

As was mentioned above, laser ceramics could also be created by hot pressing the powder obtained by grinding a doped single crystal. Such a method was applied to obtain $CaF_2:Yb^{3+}$ (3%) ceramics for laser testing. An input-output curve is shown in Fig.24 for a sample of $CaF_2:Yb^{3+}$ (3%) ceramic material, obtained by hot pressing a powder. The sample was tested in the same way as before (Fig.19-21) with an output mirror reflectivity of 95% and a 3 ms pump pulse duration. The resulting slope efficiency of 5% was found to be rather low relative to results demonstrated by hot pressed $CaF_2:Yb^{3+}$ ceramic samples. The measured oscillation output pulse duration is also shown as an inset in Fig.24. As can be seen from the figure, the output pulse was about 2 ms long and delayed about 1 ms from the laser diode pump pulse.

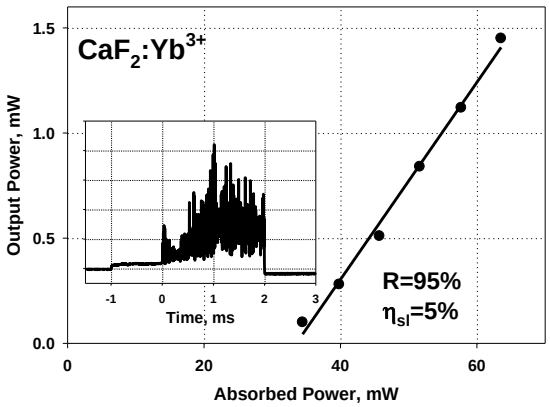

Fig.24 Input-output characteristics of a $CaF_2:Yb^{3+}$ sample formed by hot pressing a single crystal power under laser diode pumping and temporal behavior of the oscillation pulse.

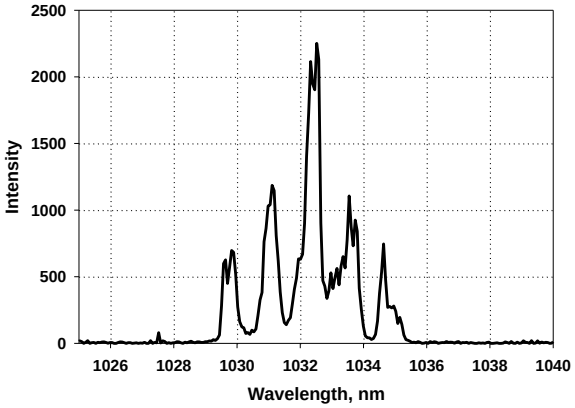

Fig.25 Oscillation spectrum of $CaF_2:Yb^{3+}$ ceramic sample.

The oscillation spectrum of CaF_2:Yb^{3+} ceramics formed by hot pressing a single crystal powder is presented in Fig.25 at the maximum pump level. As can be seen from the figure, the output oscillation spectrum is rather wide with maximum of about 1032.5 nm.

5. Nd^{3+} ions doped fluoride crystals and ceramics.

As was shown above, the clustering of Yb^{3+} ions in fluorides is a positive thing. For the case of Nd^{3+} doping of fluorides, a different situation is observed. In Fig.26, decay curves of Nd^{3+} ions in SrF_2 are presented for different excitation and detection wavelengths. As can be seen from the figure, the shape of the decay curve is changed from practically single exponential for excitation at 789 nm to double exponential for excitation at 793 nm. The reason for the difference can be found by looking at the low temperature absorption spectra of Nd^{3+} ions in SrF_2, Fig.27. As can be seen from this figure, for low concentrations of Nd^{3+} (0.5%) and rather small amounts of Nd^{3+} ion clustering, a high symmetry tetragonal absorption peak (so-called L-centers (see Fig. 9)) at 789 nm can be observed. When the concentration of Nd^{3+} is increased in SrF_2 above 0.8%, fast growth of the clustered Nd^{3+} optical centers (paired cluster - so called M-center (see Fig.9)) is observed based on the growth of the absorption at 793 nm in Fig.27. From Fig.27 for a Nd^{3+} concentration of 1%, the 793 nm absorption line of the M-centers is already stronger than the absorption line at 789 nm of the L-centers. That's why mostly tetragonal unquenched L-centers are excited with 789 nm pumping while both L- and paired M-centers are excited with 793 nm excitation at room temperature for a Nd^{3+} concentration of 0.5% (see Fig.27).

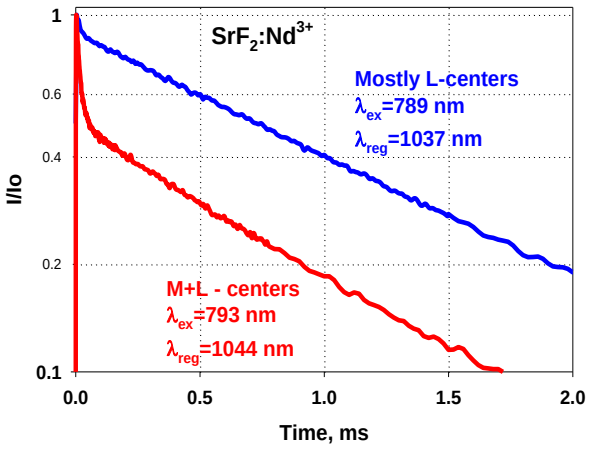

Fig.26 Decay curves of Nd^{3+} ions for different excitation and detection wavelengths

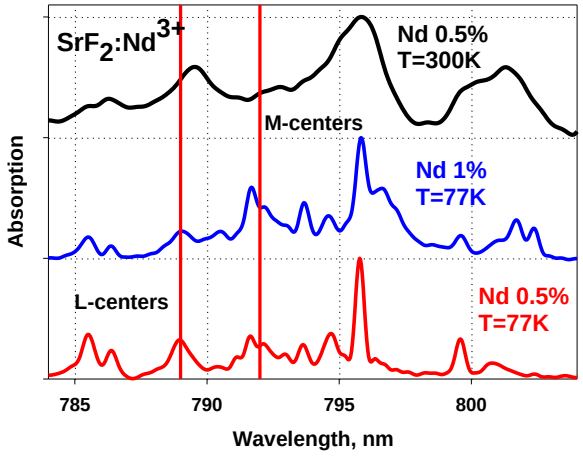

Fig.27 Low temperature absorption spectra of Nd^{3+} ions in SrF_2 for different concentrations

In Fig. 28, the initial part of decay curve for Nd^{3+} ions excited by 793 nm in a SrF_2 crystal is shown with an increased resolution. As can be seen from the figure, the decay curve has a clear

double component structure which can be approximated by the sum of two exponents (shown by the red solid line in Fig.28) with the initial fast decay having a lifetime of 18 μs and the slower decay in the tail having a much longer lifetime of 1.1 ms. The short decay time of 18 μs is attributed to quenching of the fluorescence of paired Nd^{3+} M-centers by strong ion-ion pair interactions. To test this theory of lifetime shortening, a SrF_2-LaF_3 solid solution was prepared. The advantage of this solid solution is that Nd-La pairs are predominately formed but due to the optical inactivity of the La^{3+} ions, no quenching occurs. In Fig.29, the decay curve of Nd^{3+} ions in a SrF_2-LaF_3 ceramic is shown with a characteristic decay time of 620 μs for Nd^{3+} concentrations twice as high in the range of 1%. This lifetime is much longer than the 18 μs observed for Nd-Nd paired centers and is much closer to the lifetime of unquenched, high symmetry, single L-centers in SrF_2.

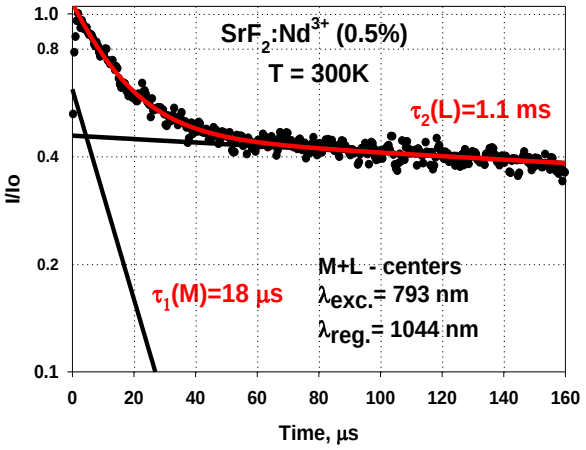

Fig.28 Double exponential decay curve of Nd^{3+} ions in SrF_2.

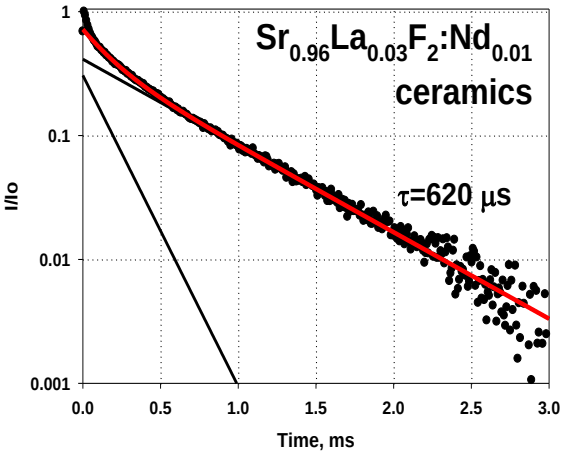

Fig.29 Decay curve of Nd^{3+} ions in SrF_2-LaF_3 ceramics with unquenched Nd-La paired centers

Using time and spectral resolution, the individual fluorescence spectra of high symmetry tetragonal L- and paired M-centers were measured. The results are shown in Fig.30. As can be seen from the figure, the fluorescence spectra of different Nd^{3+} optical centers have different spectral positions for the fluorescence maxima. L-centers have a short wavelength maximum at 1037 nm (with second maximum at 1044 nm) while the fluorescence maximum of paired M-centers is observed to occur at 1045 nm (with second maximum at 1060 nm). In Fig.31, the fluorescence spectrum of Nd-La paired centers in a SrF_2-LaF_3 ceramic is presented along with the fluorescence spectrum of paired Nd-Nd M-centers in SrF_2 ceramic. As can be seen from the figure, the Nd-La paired M-center has a shape and spectral position very similar to that observed for the Nd-Nd paired M-center.

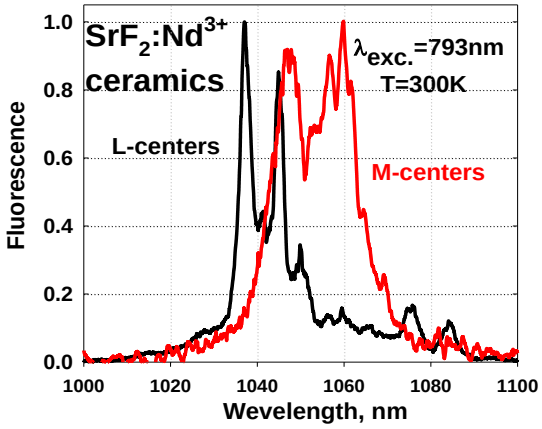

Fig.30 Fluorescence spectra of Nd^{3+} L and M optical centers in SrF_2.

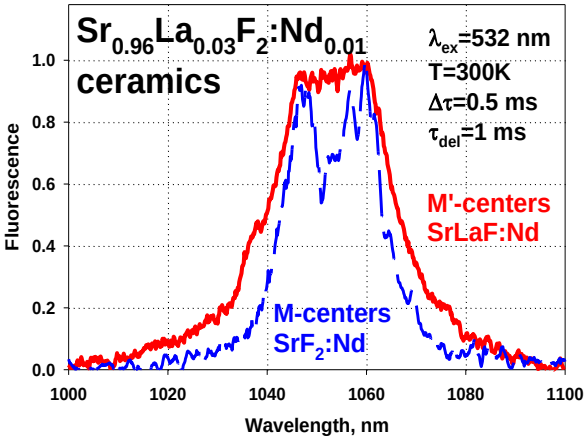

Fig.31 Fluorescence spectra of Nd-La and Nd-Nd paired centers in SrF_2-LaF_3 and SrF_2 ceramics.

From a lasing point of view, the sensitivity of the spectroscopic properties of Nd^{3+} ions on the excitation wavelength (due to excitation of primarily one type of Nd^{3+} optical center) results in different oscillation spectra for even small shifts of the laser diode operating wavelength. This oscillation wavelength dependence is shown in Fig.32 for laser diode oscillation at both ~789 nm and ~793 nm, i.e., the wavelengths where (as was discussed previously) mostly high symmetry L-centers and paired M-centers are pumped, respectively. Thus for low levels of pumping, a 4 nm shift of the laser diode oscillation wavelength from 789 to 793 nm results in a switch of the SrF_2:Nd^{3+} lasing line from 1037 nm (fluorescence maximum of L center) to 1045 nm (fluorescence maximum of M center) (see Fig.30). With respect to the efficiency of lasing, the excitation of quenched M-centers, which have a low quantum yield (ratio of the total number of fluorescence photons from an excited electronic level per excitation photon, i.e., a value of 1 is obtained if each excitation photon produces one fluorescent photon), results in a lower oscillation efficiency due to a strong loss of excitation energy during fast nonradiative interactions in Nd-Nd pairs than would be the case if mostly unquenched L-centers were pumped. This is illustrated in Fig.33 where the oscillation properties of SrF_2:Nd^{3+} ceramics are shown for diode pumping into the Nd^{3+} ions absorption maximum (see Fig. 27 for example) at 795 nm where both types of Nd^{3+} optical centers are excited and for diode pumping at 790 nm where mostly L-centers are excited. As can be seen from the figure, the excitation of mostly unquenched L-centers results in an increase in the slope efficiency from 16.5% to 19% even though the pump absorption is lower in this case.

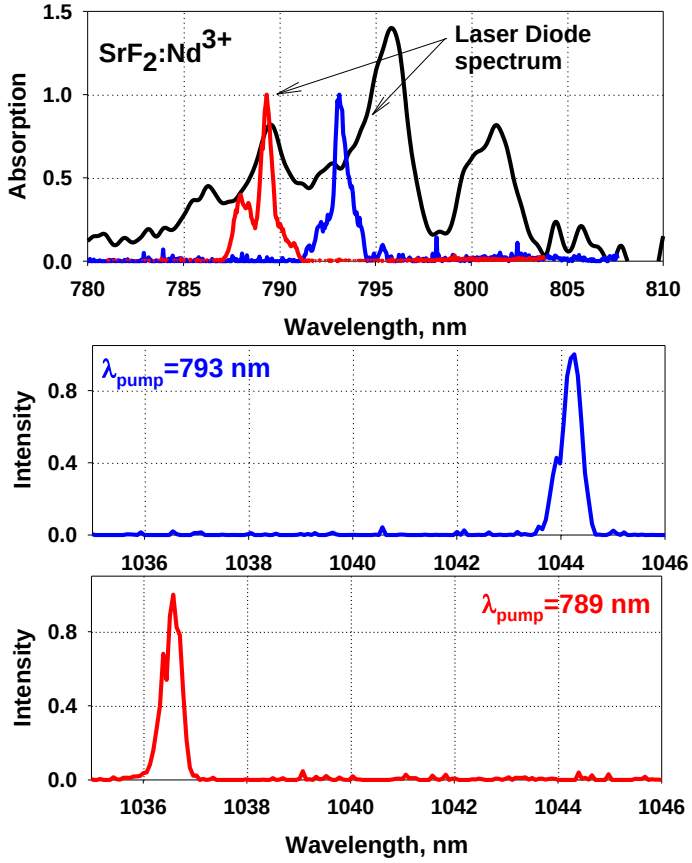

Fig.32 Oscillation spectra of $SrF_2:Nd^{3+}$ for two excitation wavelengths of the laser diode pump.

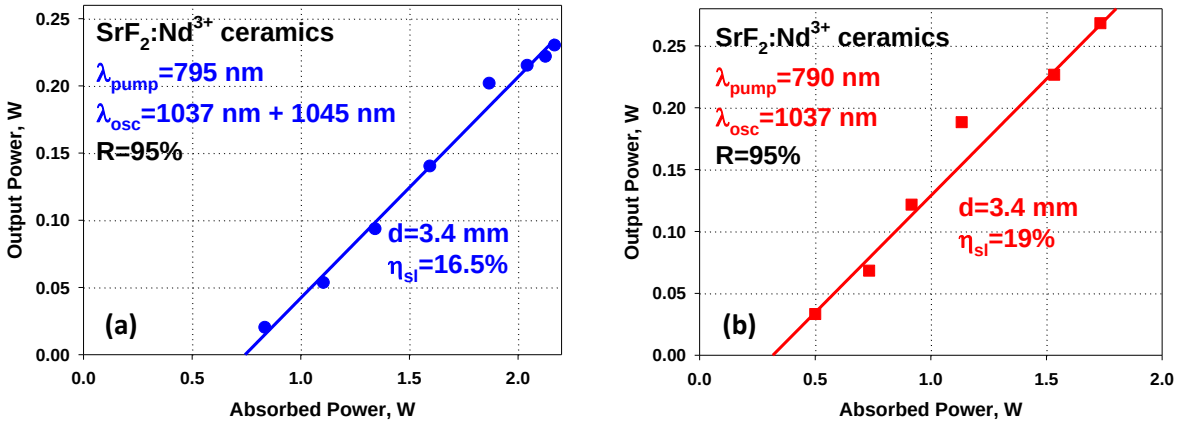

Fig.33 Output power versus pump power characteristics of $SrF_2:Nd^{3+}$ ceramics for laser diode pumping into the absorption maximum of: (a) 795 nm for excitation of both L- and M-centers and (b) 790 nm for excitation of mostly Nd^{3+} L-centers.

The situation can be improved when a SrF_2-LaF_3 solid solution is used. As was discussed above, the formation of paired Nd-Nd M-centers in SrF_2 rapidly increases for Nd^{3+} concentrations exceeding 0.8%. Even at a Nd^{3+} concentration level of 0.5%, the number of paired Nd-Nd M-centers relative to the entire number of Nd^{3+} centers is enough to obtain oscillation on only this

type of Nd^{3+} optical center. The usage of a SrF_2-LaF_3 solid solution enables higher Nd^{3+} concentrations since the formation of pair centers are not an issue since mostly Nd-La pairs are formed which are not quenched. Because of higher obtainable concentrations of Nd^{3+} in a SrF_2-LaF_3 solid solution, higher pump absorptions and higher levels of laser output power are obtained for a sample pumped at the ~795 nm absorption maximum. This is illustrated in Fig.34 where the input-output characteristic of a SrF_2-LaF_3 ceramic doped with 1% of Nd^{3+} is shown. When the Nd^{3+} concentration was doubled in a SrF_2-LaF_3 solid solution to 1%, an increase in the ~795 nm pump absorption by a factor of two relative to SrF_2:Nd^{3+} (0.5%) was obtained with a slope efficiency very similar to what was obtained when Nd^{3+} L-centers were pumped with 790 nm (see Fig.33). The result was an increase in the maximum output power from 250 to about 800 mW. This result seems rather promising since fully optimized, diode pumped YAG:Nd has a reported maximum slope efficiency of about 40%.

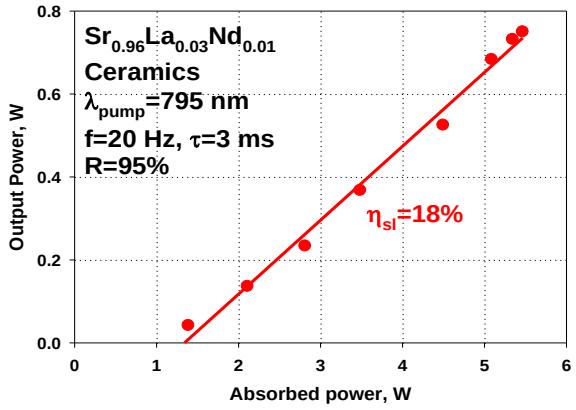

Fig.34 Input-output characteristics of SrF_2-LaF_3 ceramics under 795 nm laser diode pumping.

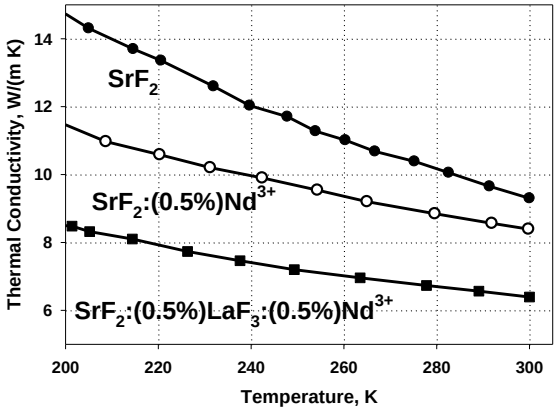

Fig.35 Thermal conductivity of pure SrF_2, SrF_2 doped with 0.5% of Nd^{3+} and SrF_2-LaF_3:Nd^{3+}.

Thus, usage of a SrF_2-LaF_3 solid solution helps to remove Nd-Nd quenching and the associated nonradiative losses due to the formation of unquenched Nd-La pairs. To ensure that Nd-La pairs predominate in a SrF_2-LaF_3 solid solution, a LaF_3 concentration 2-3 times higher than that associated with Nd^{3+} is usually used to increase the probability of Nd-La pairs formation. Because higher concentrations of Nd^{3+} are possible in the host, an increase in the pump absorption efficiency is obtained. Also for a La content less than 20%, the cubic structure of the matrix in such solid solutions is preserved which enables obtainment of high optical quality ceramics. The downside associated with this is a drop in the SrF_2-LaF_3 solid solution thermal conductivity as shown in Fig.35 where the temperature dependence of the thermal conductivity for nominally pure SrF_2 is compared to 0.5% Nd^{3+} doped SrF_2 and a 0.5% Nd doped SrF_2-0.5%

LaF_3 solid solution. As can be seen from the figure at room temperature, a decrease in the thermal conductivity of the SrF_2-LaF_3 solid solution is observed. It must be mentioned, though, that the resulting thermal conductivity is still above 6 W/(m K) which is very close to that of the well-known $YLiF_4$:Nd crystal.

To evaluate the optical losses in SrF_2:Nd^{3+} and SrF_2-LaF_3:Nd^{3+} ceramics, the pump input-laser output curves for different reflectivities of the output mirror were measured. These dependencies for the SrF_2:Nd^{3+} ceramic are shown in Fig.36. The lasing threshold versus the reflectivity of the output mirror for SrF_2:Nd^{3+} and SrF_2-LaF_3:Nd^{3+} ceramics are presented in Fig.37 with the optical losses associated with both samples evaluated to be about 3%.

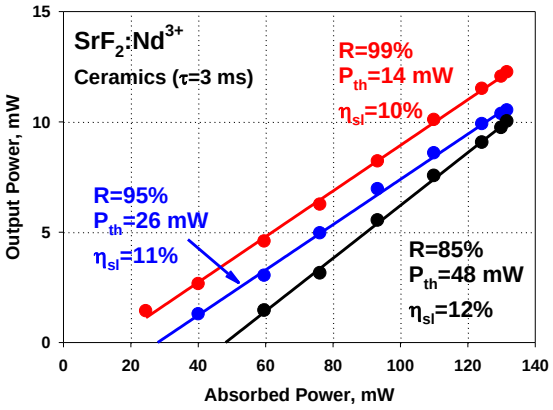

Fig.36 Input-output characteristics of SrF_2:Nd^{3+} ceramics for different output mirror reflectivities.

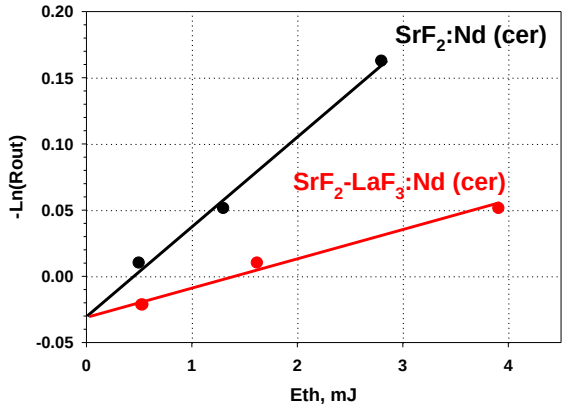

Fig.37 Evaluated optical losses in SrF_2:Nd^{3+} and SrF_2-LaF_3:Nd^{3+} ceramics.

The high optical quality associated with SrF_2:Nd^{3+} ceramics also allowed obtainment of oscillations when the sample was turned along the long axis where the thickness was approximately 3 times larger (i.e., 12.4 mm instead of 3.4 mm). A pump wavelength of 790 nm was used and the resulting pump input-laser output characteristics are shown in Fig.38. As can be seen from the figure, because of a reduced match between the pump volume and the laser cavity mode, a lower slope efficiency of approximately 14% was obtained. The longer absorption length also enabled pumping with a standard 805 nm laser diode which does not match well with the absorption maximum of Nd^{3+} ions in SrF_2 ceramics. Because of this, a longer absorption length is necessary to obtain the desired level of pump absorption. In Fig.38, even though the absorption associated with the 805 nm pump was two times lower than that associated with the 790 nm pump, the slope efficiency obtained with the 805 nm pump was practically the same. Also, the oscillation spectra obtained with 805 nm pumping (to include up the maximum pump level) were mostly on the short 1037 nm wavelength line which is characteristic for high symmetry L-centers, Fig.39.

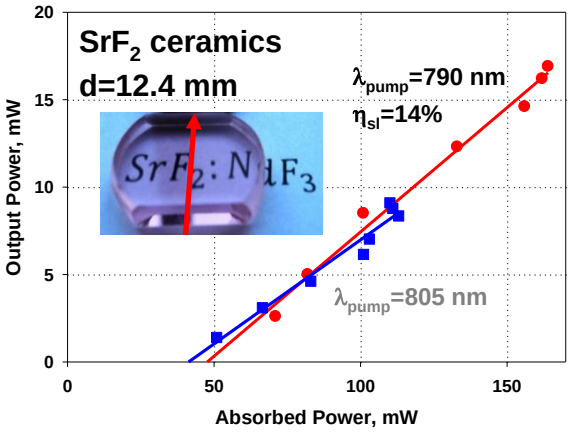

Fig.38 Input-output characteristics of $SrF_2:Nd^{3+}$ ceramics under 790 nm and 805 nm pumping

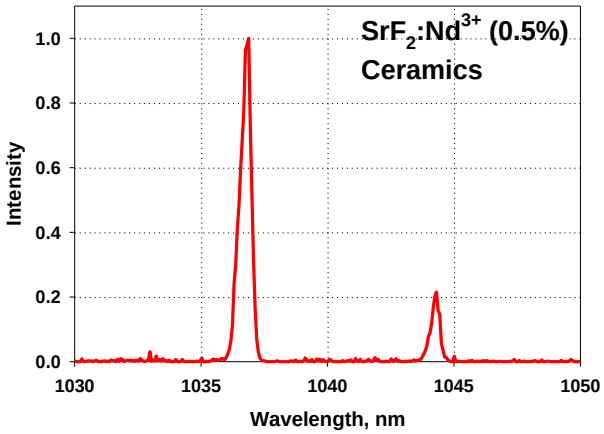

Fig.39 Oscillation spectrum of $SrF_2:Nd^{3+}$ ceramics under 805 nm laser diode pumping.

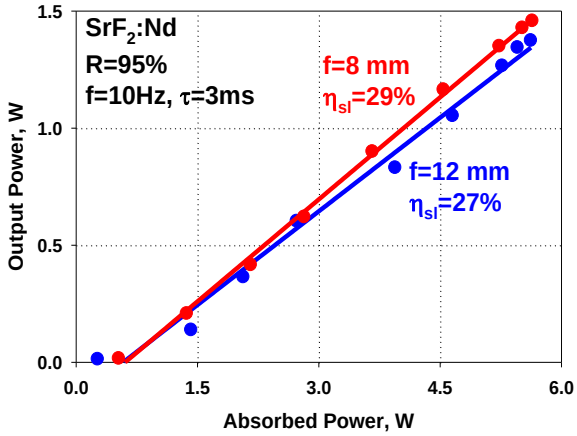

Fig.40 Optimization of the pump mode to cavity mode for the $SrF_2:Nd^{3+}$ single crystal.

To estimate the maximum lasing efficiency, a $SrF_2:Nd^{3+}$ (0.5%) crystal was specially prepared with one surface antireflection coated and the other being a dichroic mirror that was transparent at the pump wavelength while being totally reflective at the lasing wavelength. In Fig.40, the results of experiments on matching the cavity mode to the pump mode are presented. As can be seen from the increase in the slope efficiency from 27 to 29% in the figure, usage of a pump focusing lens having a shorter focal length resulted in a better match of the pump volume to the cavity mode. The maximum obtained slope efficiency in this case was not far from the best results obtained from a $YAG:Nd^{3+}$ crystal.

Unlike neodymium doped SrF_2 ceramics, switching of the oscillation wavelength was not observed with $CaF_2:Nd^{3+}$ ceramics. It should be noted that in CaF_2, clustering of Nd^{3+} ions starts at lower (0.3%) concentrations relative to what was seen with SrF_2. In Fig.41, the measured time and spectrally resolved fluorescence spectra of Nd^{3+} L and M optical centers is shown. As can be

seen from the figure, even for Nd^{3+} concentrations in CaF_2 two times lower than in SrF_2, the signal to noise ratio arising from clustered M-centers is much worse than was the case with SrF_2 ceramics because of stronger Nd-Nd quenching. Also unlike SrF_2, in CaF_2, the ceramics fluorescence maximum for both types of optical centers occurs at the same wavelength of 1046 nm. So, even when the pump wavelength was changed, oscillations were only observed at 1046 nm as shown in Fig.42.

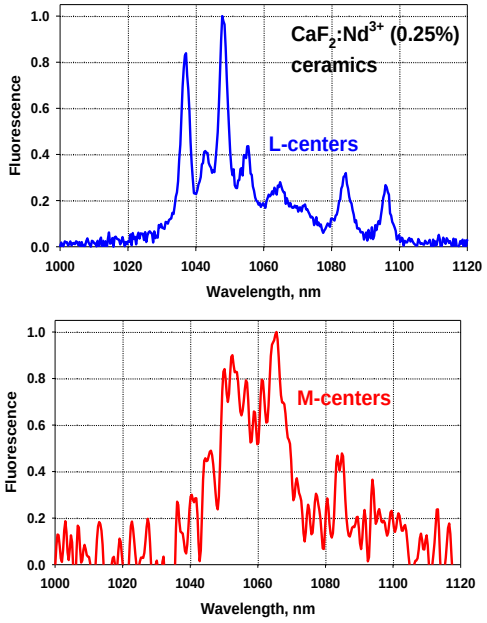

Fig.41 Fluorescence spectra for L and M-centers in CaF_2:Nd^{3+} ceramics

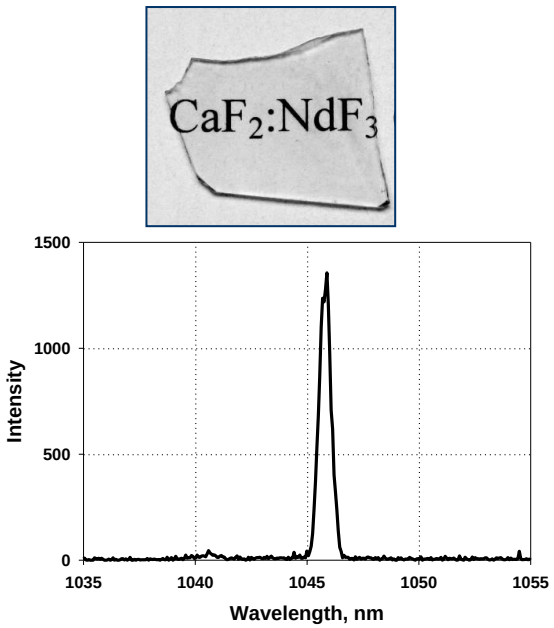

Fig.42 Oscillation spectrum of CaF_2:Nd^{3+} ceramics under laser diode pumping.

6. Pr^{3+} ions doped fluoride crystals and ceramics.

Fluoride ceramics doped with Yb^{3+} or Nd^{3+} ions were previously shown to operate in the near IR spectral region. At the same time, it is expected that optical losses in a ceramic host material caused by multiphoton absorption as well as scattering on grain boundaries, pores and inclusions should strongly increase for shorter wavelengths. From this point of view, the development and the investigation of laser ceramics which can oscillate at visible wavelengths is of great interest.

Praseodymium ions are mostly suitable for enabling laser oscillation in the visible under direct laser diode pumping. Such oscillations were previously demonstrated in oxide (YAP) and fluoride ($YLiF_4$) crystals [4,5]. Because of a suitable electronic level scheme, see Fig.43, praseodymium ions have several channels available for visible oscillations. The SrF_2 ceramic was initially chosen as the host due to the fact that RE^{3+} ion pairings in SrF_2 usually start at

higher doping concentrations relative to the CaF_2 ceramic. The fluorescence spectrum of Pr^{3+} ions in SrF_2 is shown in Fig.44 with the most intense line, in the red region, peaking at 639 nm.

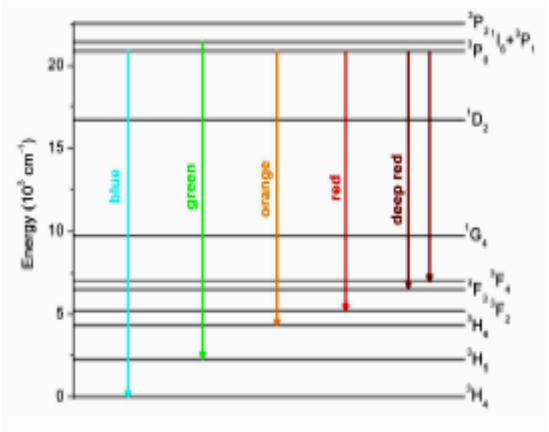

Fig.43 Pr^{3+} ion fluorescence channels in the visible spectral range

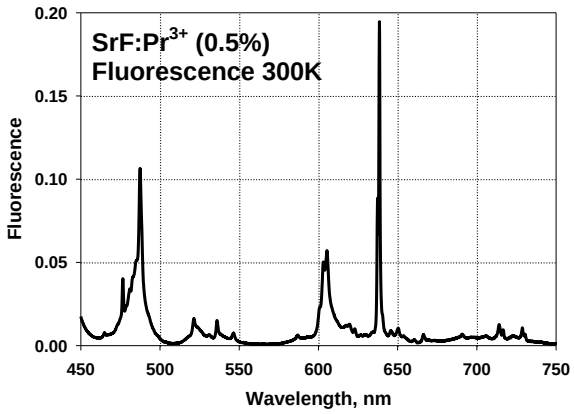

Fig.44 Pr^{3+} ion fluorescence spectrum in the visible spectral range.

To investigate the spectroscopic properties of Pr^{3+} optical centers in SrF_2, a narrow linewidth tunable laser based on a LiF crystal with F_2^+ color centers that was capable of generating short nanosecond pulses was utilized. Shown in Fig.45 is a photograph of the computer controlled LiF:F_2^+ tunable laser and shown in Fig.46 is a tuning curve of the laser in the near infrared. When frequency doubled, this tuning curve matched well the absorption lines of Pr^{3+} ions in the "blue" spectral range and was therefore utilized in spectroscopic and kinetic measurements.

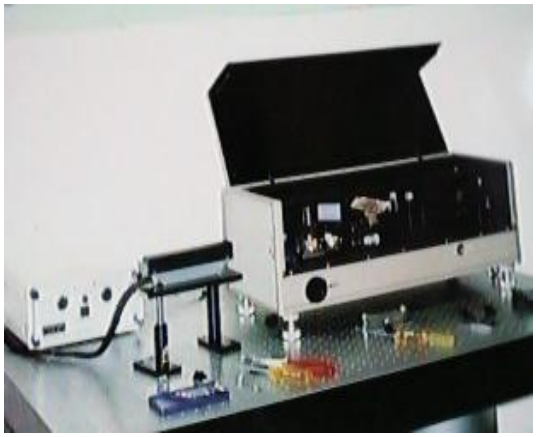

Fig.45 Optically pumped tunable laser based on a LiF crystal with F_2^+ color centers

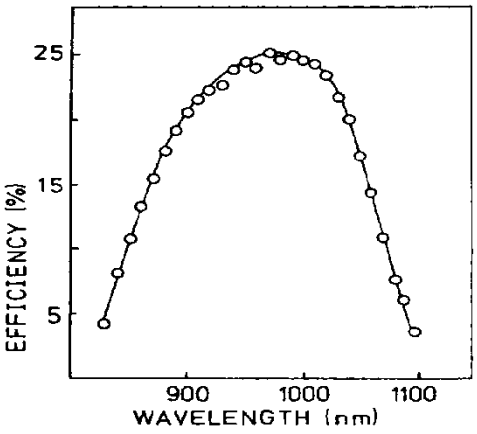

Fig.46 Tuning curve of LiF:F_2^+ color center laser.

As was shown by previous investigations, the lifetime of the $^3P_0$ state from which visible fluorescence originates (see Fig.43) in the various fluorides is quite similar and is in the range of about 40 μs (see Table 2 [6]).

Table 2 – Approximate Positions and Fluorescence Lifetimes of the $^1D_2$ and $^3P_0$ Metastable Levels in Pr-Doped Ky_3F_{10}, $LiYF_4$, and BaY_2F_8

Materials	Pr:KY_3F_{10}	Pr:$LiYF_4$	Pr:BaY_2F_8
$\nu(^3P_0)$	20 730 cm^{-1}	20 860 cm^{-1}	20 840 cm^{-1}
$\tau(^3P_0)$	33.5 μs	43.5 μs	42.5 μs
$\nu(^1D_2)$	16 670 cm^{-1}	16 740 cm^{-1}	16 650 cm^{-1}
$\tau(^1D_2)$	92.5 μs	205 μs	175 μs

Measurement of the lifetimes of SrF_2:Pr^{3+} ceramics has shown that relative to other fluorides, optical centers having lifetimes twice as long have been observed. Similar to Nd^{3+} doping, an essential residual structure, even at room temperature, is observed in the absorption spectrum of SrF_2:Pr^{3+} ceramics, especially for lower (0.3%) Pr^{3+} concentrations, Fig.47. The situation is similar to the case of SrF_2:Nd^{3+} ceramics in that the excitation of two closely lying absorption maxima in SrF_2:Pr^{3+} ceramics results in two different decay curves which could also be attributed to high symmetry L-like optical centers with a longer lifetime and low symmetry paired M-like optical centers having a shorter lifetime (see Fig.48). Unlike SrF_2:Nd^{3+}, though, the difference in lifetimes is not as large (about a factor of 2) and looks more like the difference in lifetimes between a high symmetry single L-center and a Nd-La paired M-center. It should be mentioned that the spectral distance between the two absorption maxima is only about 4 nm (438 nm and 442 nm) and is very similar to that observed for Nd^{3+} ions (789 nm and 793 nm) in SrF_2 ceramics. The measured lifetime of 43 μs was similar to the lifetime of the $^3P_0$ state in other fluorides. The additional long 108 μs decay is characteristic of the SrF_2 fluoride. Despite the residual structure, the absorption band in the "blue" spectral region is rather broad and is well suited for pumping with standard 444 nm GaInN laser diodes.

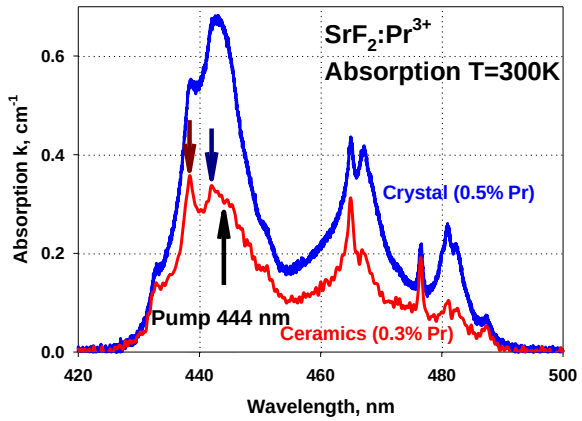

Fig.47 Absorption spectra of Pr^{3+} ions in SrF_2 for crystal and ceramics with different Pr^{3+}. concentrations

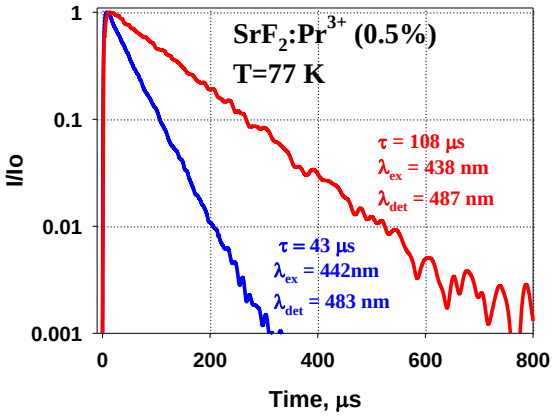

Fig.48 Decay curves of Pr^{3+} ions measured for different excitation wavelengths.

To measure an individual fluorescence spectrum for the two types of observed optical centers, excitation into the $^3P_1$ state was used. Using the time resolved technique, the fluorescence spectrum for high symmetry centers (with a longer lifetime of 108 μs) was obtained using a 465 nm excitation wavelength as shown in Fig.49. The fluorescence spectrum for the low symmetry centers (with a shorter lifetime of 43 μs) was obtained with 467 nm excitation and is shown in Fig.50.

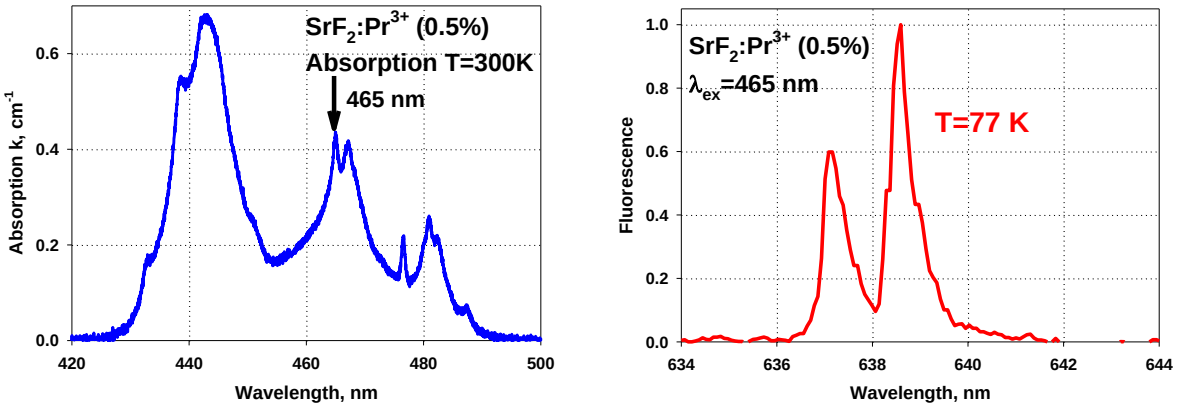

Fig.49 Fluorescence spectra of Pr^{3+} ions in high symmetry optical centers (t=108 μs) on the $^3P_0$ -$^3F_2$ transition of the SrF_2 crystal at liquid nitrogen temperatures for 465 nm excitation.

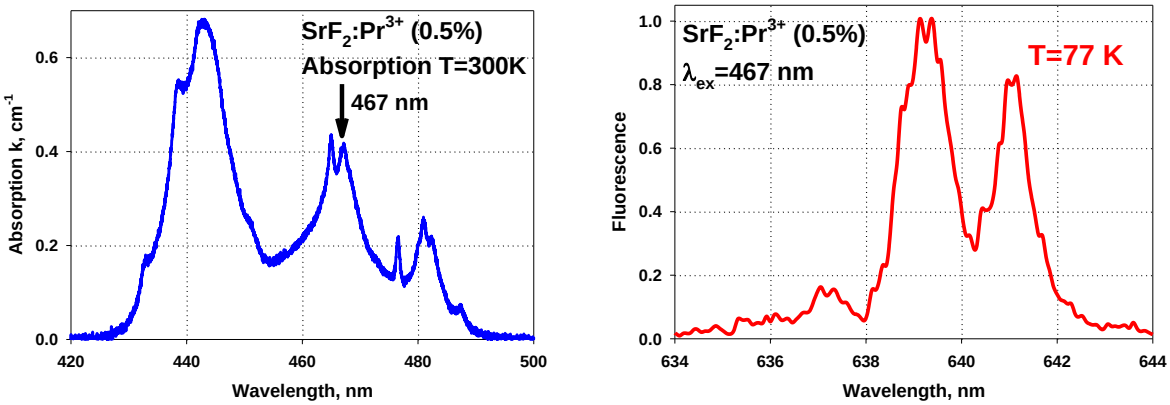

Fig.50 Fluorescence spectra of Pr^{3+} ions in lower symmetry paired optical centers (t=43 μs) on the $^3P_0$- $^3F_2$ transition of the SrF_2 crystal at liquid nitrogen temperatures for 467 nm excitation.

As can be seen from the fluorescence spectra, the positions of the fluorescence maxima for the different Pr^{3+} ions optical centers is close to what was observed in CaF_2:Nd^{3+} ceramics where the two fluorescence maxima coincided well with each other. This should result in a weak dependence of oscillation spectrum on the excitation wavelength.

Lasing properties of SrF_2:Pr^{3+} ceramics were tested by pumping with a GaInN laser diode that had a central emission wavelength of 444 nm and a maximum output power of 1W. Because the

ceramic sample being tested was about 3 mm thick with a Pr^{3+} concentration of 0.3%, about 9% of the 444 nm pump radiation was absorbed. The single crystal sample on the other hand, had a thickness of 5 mm and a Pr^{3+} concentration of 0.5% which resulted in a pump absorption of 26%. For the experiments, a hemispherical cavity was formed by the plane input coupling mirror which had an anti-reflection coating at the pump wavelength but was highly reflective around 640 nm ($^3P_0$-$^3F_2$ transition of the Pr^{3+}-ion) and an output mirror which had a radius of curvature of 50 mm. The pump beam was focused into the active medium by a lens with a focal length of 40 mm and laser oscillations were obtained in CW mode without special cooling of ceramic sample. The pump input-laser output characteristics for SrF_2:Pr^{3+} ceramics with different transmittances of the output coupler are shown in Fig.51. As can be seen from the figure, a slope efficiency of about 9% was realized. Using data for the oscillation thresholds of the different output couplers, cavity losses were estimated to be about 4% (see Fig.52) using the Findlay-Clay method [7] which is quite similar to the loss value of about 3% obtained for case of SrF_2:Nd^{3+} ceramics (see Fig.37). Thus switching to visible spectral range is not accompanied by significant growth in the optical losses of SrF_2 ceramics.

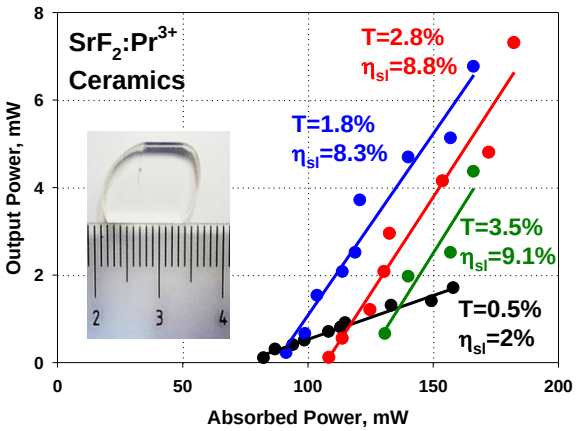

Fig.51 Input-output characteristics of SrF_2:Pr^{3+} ceramics for different output mirror transmittances.

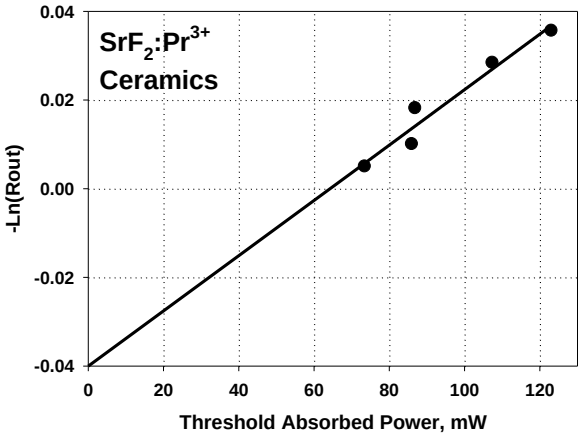

Fig.52 Evaluated optical losses in SrF_2:Pr^{3+} ceramics.

In Fig.53, the dependence of slope efficiency of the oscillations on the transmittance of the output mirror is plotted. As can be seen from the figure, an output mirror transmittance of about 2-3% seems to be close to the optimal value. In Fig.54, a comparison of the laser properties of SrF_2 single crystal and ceramics are shown under similar conditions. As can be seen from the figure, higher concentrations of Pr^{3+} along with larger sample thicknesses result in higher pump absorption in the single crystal and thus higher output power. At the same time, the slope efficiencies of both the single crystal and ceramics were practically the same while the oscillation threshold of ceramics was lower.

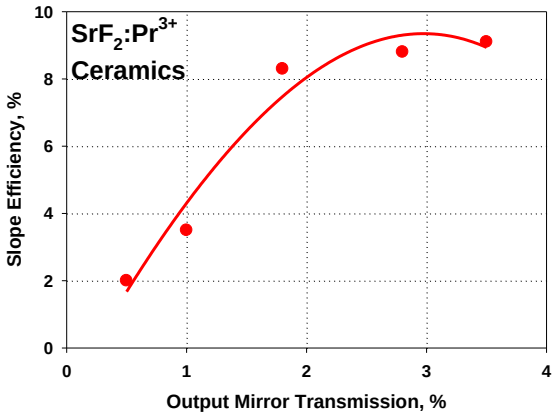

Fig.53 Lasing slope efficiency of $SrF_2:Pr^{3+}$ ceramics for different output mirror transmittances.

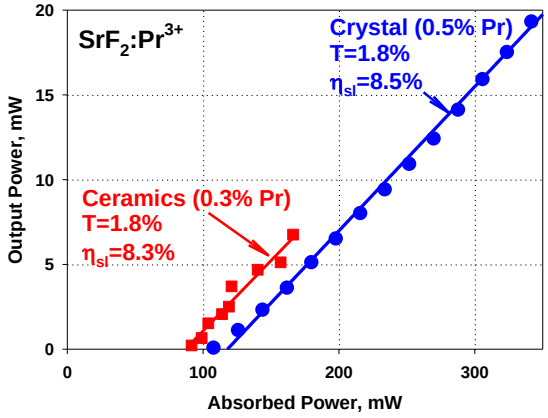

Fig.54 Comparison of input-output characteristics of $SrF_2:Pr^{3+}$ ceramics and single crystal samples for an output mirror reflectivity of 98.2%.

The 444 nm GaInN pump laser diode matches the absorption maximum of Pr^{3+} ions in SrF_2 well as can be seen in Fig.54. At the same time, this pump wavelength matches the position of the absorption maximum of the lower symmetry Pr^{3+} optical center better. It also should be noted that the 443 nm absorption peak grows faster than the 438 nm peak with an increase in the concentration of Pr^{3+} from 0.3% to 0.5% (see Fig.55). The measured oscillation spectra of Pr^{3+} ions for different Pr^{3+} concentrations are shown in Fig.56. As can be easily seen from the figure, the oscillation spectra could be assumed to be a superposition of two oscillating lines quite analogous to the situation of Nd^{3+} ions in SrF_2. Though in case of Pr^{3+} ions, the maxima of the oscillating lines lie close together and are separated by approximately 1 nm. As can be seen from Fig.56, the oscillation spectra could be fit with a narrow line peaking at ~638.5 nm and a line with twice the width peaking at ~639.5 nm. The positions of these two maxima and line widths fit well with the fluorescence maxima observed for high symmetry (638.5 nm) and low symmetry (639.5 nm) Pr^{3+} optical centers. It also follows from Fig.56 for a lower Pr^{3+} concentration of 0.3% that the short wavelength oscillation maximum (638.5 nm) attributed to high symmetry centers is more intense than longer wavelength (639.5 nm) maximum attributed to lower symmetry centers. The inverse situation is observed for a Pr^{3+} concentration of 0.5% where the intensity of the longer wavelength line prevails. For 444 nm excitation, both Pr^{3+} optical centers are excited and participate in laser operation as was the case with Nd^{3+} doped materials where excitation into the absorption maximum resulted in oscillation of both Nd^{3+} optical centers.

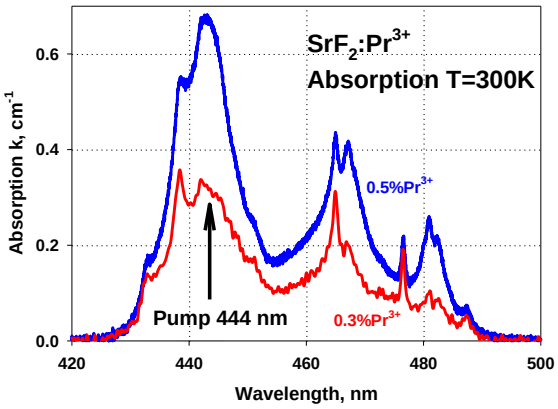

Fig.55 Absorption spectra of SrF_2 with Pr^{3+} ion concentrations of 0.3% and 0.5%

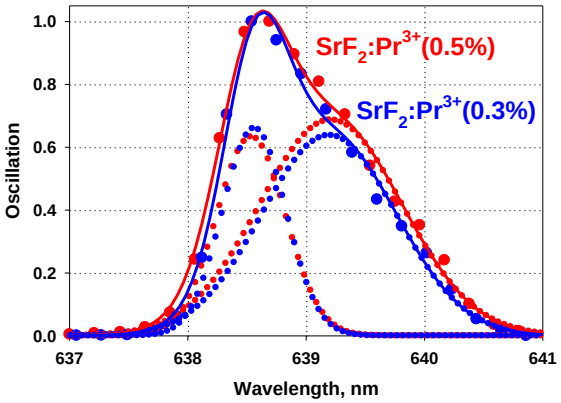

Fig.56 Oscillation spectra of Pr^{3+} ions in SrF_2 for two Pr^{3+} concentrations and their fit.

As was discussed above, fluorescence quenching of Nd^{3+} ions in paired M-centers resulted in a lower laser efficiency when both types of optical centers were pumped. The suggested solution was to use a SrF_2-LaF_3 solution to form non-quenched Nd-La ion pairs. The oscillation spectrum of Pr^{3+} ions was also found to consist of two lines attributable to two Pr^{3+} ion optical centers, one of which was characterized by a lifetime half as long. To evaluate the effect of adding La to SrF_2:Pr^{3+}, a SrF_2-LaF_3:Pr^{3+} crystal was synthesized and the lifetime of the Pr^{3+} ion was measured, Fig.57. As can be seen from the figure, the decay is single exponential with a measured lifetime of 45 μs which matches well with the lifetime of 43 μs for paired Pr^{3+} optical centers in SrF_2. This means that unlike Nd^{3+} ion pairs, the fluorescence of paired Pr^{3+} centers is not quenched. Again the price for LaF_3 doping is a decrease in the thermal conductivity as shown in Fig.58. As can be seen from the figure, a doping level of LaF_3 of 1% decreases the thermal conductivity at room temperature by approximately 20%. Also as can be seen from the figure, a doping level of Pr^{3+} of 1% causes an even stronger (~30%) drop in the thermal conductivity. Even so, the thermal conductivity at room temperature exceeds 6 W/(m K) in this case (or in case of 0.5% of LaF_3 and 0.5% of PrF_3).

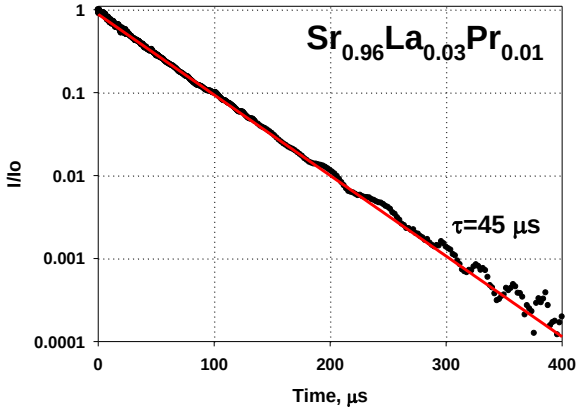

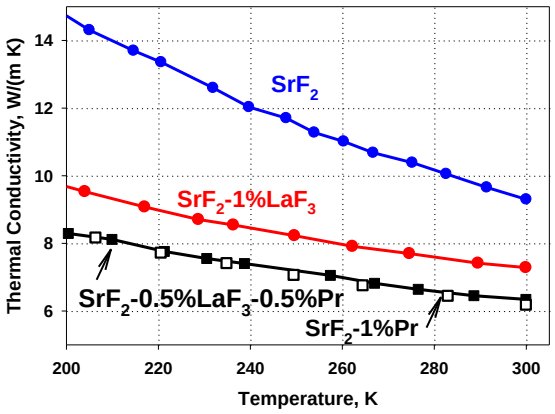

Fig.57 Decay curve of Pr^{3+} paired centers in the $Sr_{0.96}La_{0.03}Pr_{0.01}$ crystal.

Fig.58 Measured thermal conductivity for nominally pure SrF_2 and the SrF_2-1%LaF_3 solid solution doped with Pr^{3+}.

Thus, the addition of a small amount of LaF_3 to SrF_2 has little impact since the fluorescence of Pr^{3+} ions in paired centers is not quenched. A different situation is observed when much higher concentrations of LaF_3 are used. As was mentioned previously, the cubic structure of the resulting solid solution is preserved for concentrations of LaF_3 below 20%. To investigate the spectroscopic and laser properties of Pr^{3+} ions in solid solutions having a large (14%) concentration of LaF_3, the $Ca_{0.75}Sr_{0.1}La_{0.14}Pr_{0.01}$ crystal was synthesized. The measured fluorescence spectrum of Pr^{3+} ions in this solid solution is shown in Fig.59 together with the fluorescence spectrum of Pr^{3+} ions in LaF_3 crystal. As can be seen from the figure, the positions of fluorescence maxima in LaF_3 and the solid solution are quite similar with significant inhomogeneous broadening of the fluorescence lines in the solid solution. The measured decay curves of the Pr^{3+} ions (see Fig.60) in the $Ca_{0.75}Sr_{0.1}La_{0.14}Pr_{0.01}$ solid solution have been found to have lifetimes of about 40 μs which are close to the lifetimes of the Pr-La centers in the SrF_2-LaF_3 solid solution with a low LaF_3 content as well as the LaF_3 crystal. Thus, the $Ca_{0.75}Sr_{0.1}La_{0.14}Pr_{0.01}$ solid solution demonstrates spectroscopic properties close to those of the LaF_3 crystal. Of note, the LaF_3 crystal is anisotropic due to a hexagonal crystal structure and up to now has not been available in a ceramic form. The cubic $Ca_{0.75}Sr_{0.1}La_{0.14}Pr_{0.01}$ solid solution, on the other hand, enables a laser ceramic with a shifted fluorescence maximum similar to that of the LaF_3 crystal.

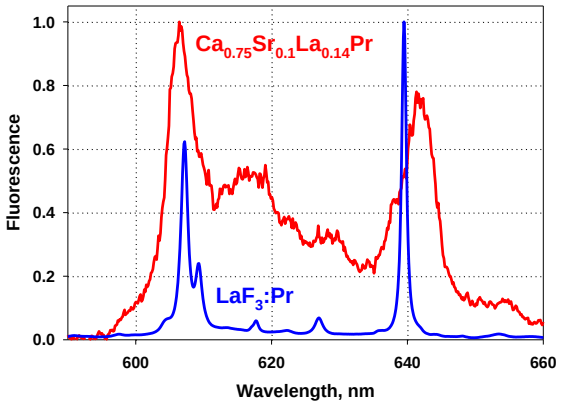

Fig.59 Fluorescence spectra of $Ca_{0.75}Sr_{0.1}La_{0.14}Pr_{0.01}$ and LaF_3:Pr crystals.

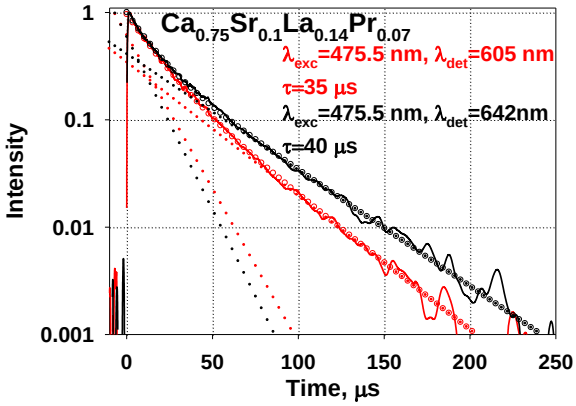

Fig. 60. Decay curves of Pr^{3+} ions measured at the two fluorescence maximums of 605 nm and 642 nm.

The same pump configuration and cavity that was used to investigate oscillations of $SrF_2:Pr^{3+}$ was also used to investigate lasing properties of the $Ca_{0.75}Sr_{0.1}La_{0.14}Pr_{0.01}$ solid solution. Due to the high LaF_3 content as well as the twice higher (1%) Pr^{3+} concentration, the thermal properties of the $Ca_{0.75}Sr_{0.1}La_{0.14}Pr_{0.01}$ solid solution were significantly worse than those associated with $SrF_2:Pr^{3+}$ and true CW operation was not realized. In pulsed mode, oscillations were obtained with a repetition rate up to 500 Hz. For a repetition rate of 500 Hz, lasing was thermally terminated for pulse durations above 400 μs. Oscillograms of the oscillation pulse for two different pump pulse durations of 200 and 300 μs are shown in Fig.61. As can be seen in the figure, even for a pulse duration of 300 μs, sample heating that occurred toward the end of the pump pulse made the used cavity unstable (due to strong thermal lensing) and only separate oscillation spikes could be observed. The result is a dependence of oscillation threshold and lasing efficiency on the pump pulse duration as is shown in Fig.62. The lower lasing efficiency in the case of a "long" 300 μs pump pulse is caused by a partial thermal termination of oscillations after approximately 200 μs of the pump pulse, Fig.61. The remainder of the 100 μs of the 300 μs pump pulse was less useful and only caused additional heating of the sample. Reduction of the pump pulse duration to 200 μs resulted in lower heating, a better cavity stability, a more effective use of the pump pulse as well as a small increase in the slope efficiency from 2% to 3%. The oscillation threshold was not affected and was decreased 1.5 times in accordance with a 1.5 times difference in pump pulse duration (i.e., absorbed pump power also decreased 1.5 times).

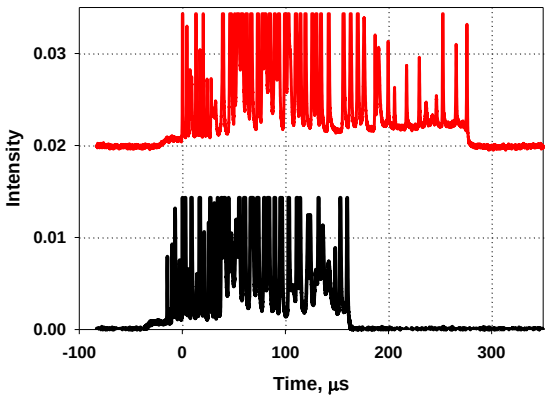

Fig.61 Oscillograms of the $Ca_{0.75}Sr_{0.1}La_{0.14}Pr_{0.01}$ solid solution oscillation pulses for pump pulse durations of 300 μs and 200 μs.

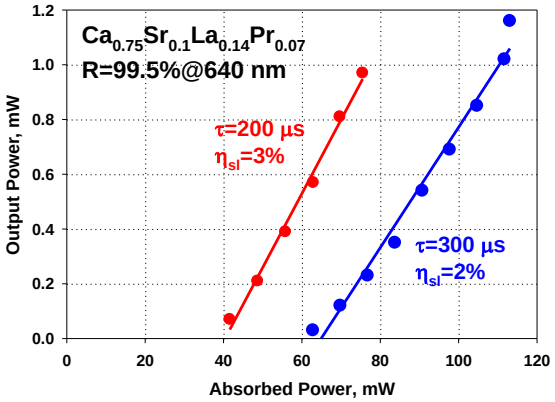

Fig.62 Input-output characteristics of the solid solution $Ca_{0.75}Sr_{0.1}La_{0.14}Pr_{0.01}$ under pumping with GaInN blue diode with different pump pulse durations.

The oscillation spectrum of the $Ca_{0.75}Sr_{0.1}La_{0.14}Pr_{0.01}$ solid solution (see Fig. 63), acquired under the same experimental conditions utilized for the $SrF_2:Pr^{3+}$ crystal, shows a 3 nm shift to the

longer wavelength of 642 nm which corresponds to the second fluorescence maximum of Pr^{3+} ions in the $Ca_{0.75}Sr_{0.1}La_{0.14}Pr_{0.01}$ solid solution (see Fig.59). Unfortunately the cavity mirrors had very low reflection at 612 nm, the most intensive fluorescence line in the $Ca_{0.75}Sr_{0.1}La_{0.14}Pr_{0.01}$ solid solution. Nevertheless, a weak oscillating line was observed for this fluorescence maximum as shown in Fig.63.

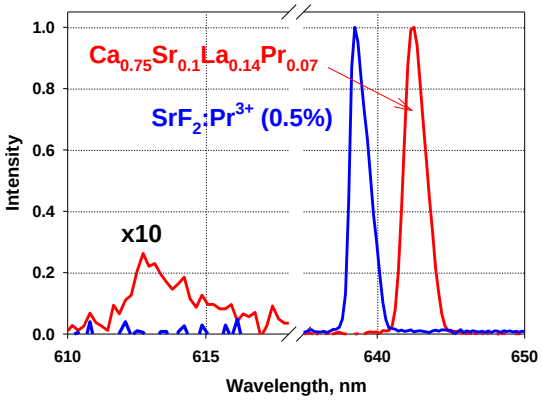

Fig.63 Oscillation spectra of $Ca_{0.75}Sr_{0.1}La_{0.14}Pr_{0.01}$ and $SrF_2:Pr^{3+}$.

7. Conclusion

The hot pressing formation technique from initial single crystals was optimized to enable obtainment of stable high optical ceramics from simple fluorides and their solid solutions doped with different RE^{3+} ions.

The spectroscopic properties of Yb^{3+} ions in fluoride ceramics of different compositions were investigated and the advantages of fluoride hosts to include a long upper laser level lifetime as well as a low minimal pumping intensity were demonstrated. The possibility of manipulating the spectroscopic and laser properties through the usage of different fluoride hosts was demonstrated and different tuning ranges for Yb^{3+} ions were realized. A slope efficiency up to 45% with respect to absorbed pump was demonstrated for the CaF_2-SrF_2:Yb^{3+} solid solution.

Fluoride CaF_2:Yb^{3+} ceramics were prepared by hot pressing single crystals and by the standard technique from powder and laser oscillations were obtained. Due to the low quantum defect of Yb^{3+} ions in CaF_2:Yb^{3+} (30%), efficient CW operation was obtained without cooling the ceramic sample.

Neodymium doped laser ceramics were obtained and the spectroscopic properties of different optical centers were determined. It was shown that selective excitation of non-quenched tetragonal optical centers resulted in a shorter oscillation wavelength with higher slope efficiency. It was also demonstrated that by using solid solutions of SrF_2-LaF_3, problems of low quantum yield arising from Nd-Nd paired optical centers were diminished enabling high oscillation efficiencies regardless of the laser diode pump wavelength.

Efficient Nd^{3+} laser oscillations with a slope efficiency up to ~20% were realized under selective laser diode pumping in SrF_2:Nd^{3+} fluoride and SrF_2-LaF_3:Nd^{3+} solid solution laser ceramics.

For an optimized SrF_2:Nd^{3+} crystal, a ~30% slope efficiency with respect to absorbed laser diode pump power was obtained which was comparable with the best result of 40% obtained for a YAG:Nd^{3+} crystal.

High optical quality SrF_2:Pr^{3+} ceramics were developed and optical losses in ceramics at the visible wavelength of 639 nm were evaluated to be on the order of the optical losses in the near infrared. Visible oscillations in red were realized in SrF_2:Pr^{3+} ceramics with slope efficiencies of up to 9%.

Praseodymium paired optical centers were shown not to be quenched and therefore do not strongly affect the lasing efficiency. Lanthanum co-doped solid solutions containing praseodymium were shown to demonstrate oscillation properties close to those of the LaF_3 crystal while preserving of the cubic structure necessary for ceramics formation.

8. References

1 S. E. Hatch, W. F. Parson, and R. J. Weagley, "Hot-pressed polycrystalline CaF_2:Dy^{2+} laser," Appl. Phys. Lett., vol. 5 (8), 153-154 (1964).

2 Fedorov P.P., Osiko V.V., Basiev T.T., Orlovskii Yu.V., Dukel'skii K.V., Mironov I.A., Demidenko V.A., Smirnov A.N., "Optical fluoride nanoceramics," Russian Nanotechnologies, vol. 2 (5-6), 95-105 (2007).

3 L.D. DeLoach, S.A. Payne, L.L. Chase, L.K. Smith, W.L. Kway, W.F. Krupke, IEEE Journal of Quantum Electronics, vol. 29, No 4 (1993).

4 M. Fibrich, H. Jelínková, J. Šulc, K. Nejezchleb, V. Škoda, "Visible cw laser emission of GaN-diode pumped Pr:$YAlO_3$ crystal", Applied Physics B: Lasers and Optics, vol. 97 (2), 363-367 (2009).

5 T. Gün, P, Metz, G. Huber, "Power scaling of laser diode pumped Pr^{3+}:$LiYF_4$ cw lasers: efficient laser operation at 522.6 nm, 545.9 nm, 607.2 nm, and 639.5 nm", Optics Letters, vol. 36 (6), 1002-1004**,** (2011).

6 Mathieu Laroche, Alain Braud, Sylvain Girard, Jean Louis Doualan, Richard Moncorge, Michel Thuau, Larry D. Merkle, "Spectroscopic investigations of the 4*f*5*d* energy levels of Pr^{3+} in fluoride crystals by excited-state absorption and two-step excitation measurements", J. Opt. Soc. Am. B, vol. 16, No. 12 (1999).

7 D. Findlay and R. A. Clay, "The measurement of internal losses in 4-level lasers," Phys. Lett. vol. 20 (3), 277-278 (1966).